The Evolution of Galaxy Structure Over Cosmic Time

Christopher J. Conselice

Center for Astronomy and Particle Theory, School of Physics and Astronomy, University of Nottingham, Nottingham, NG7 2UH, United Kingdom; email: conselice@nottingham.ac.uk

Keywords

galaxy evolution, galaxy morphology

Abstract

I present a comprehensive review of the evolution of galaxy structure in the Universe from the first galaxies currently observable at $z \sim 6$ down to galaxies observable in the local Universe. Observed changes in galaxy structures reveal formation processes that only galaxy structural analyses can provide. This pedagogical review provides a detailed discussion of the major methods used to study galaxies morphologically and structurally, including the well-established visual method for morphology; Sérsic fitting to measure galaxy sizes and surface brightness profile shapes; and nonparametric structural methods [such as the concentration (C), asymmetry (A), clumpiness (S) (CAS) method and the Gini/M_{20} parameters, as well as newer structural indices]. These structural indices measure fundamental properties of galaxies, such as their scale, star-formation rate, and ongoing merger activity. Extensive observational results demonstrate how broad galaxy morphologies and structures change with time up to $z \sim 3$, from small, compact and peculiar systems in the distant Universe to the formation of the Hubble sequence, dominated by spirals and ellipticals. Structural methods accurately identify galaxies in mergers and allow measurements of the merger history out to $z \sim 3$. I depict properties and evolution of internal structures of galaxies, such as bulges, disks, bars, and at $z > 1$ large star-forming clumps. I describe the structure and morphologies of host galaxies of active galactic nuclei and starbursts/submillimeter galaxies, along with how morphological galaxy quenching occurs. The role of environment in producing structural changes in galaxies over cosmic time is also discussed. Galaxy sizes can also change with time, with measured sizes up to a factor of 2–5 smaller at high redshift at a given stellar mass. I conclude with a discussion of how the evolving trends, in sizes, structures, and morphologies, reveal the formation mechanisms behind galaxies and provides a new and unique way to test theories of galaxy formation.

1. INTRODUCTION

Galaxy structure is one of the fundamental ways in which galaxy properties are described and by which galaxy evolution is inferred. There is a long history of the development of this idea, which began with the earliest observations of galaxies, and continues up to the modern day as one of the major ways we study galaxies. This review gives a detailed description of the progress made up to late 2013 in using galaxy structure to understand galaxy formation and evolution. It is meant to be used as a primer for obtaining basic information from galaxy structures, including how they are measured and applied through cosmic time.

The introduction to this review first gives an outline of the basic events in the history of galaxy morphology and structure analyses, whereas the second part of the introduction describes how galaxy structure fits into the general picture of galaxy formation. I also give a detailed description of the goals of this review at the end of the introduction.

1.1. Historical Background

Galaxy morphology has a long history, one that even predates the time when we finally knew galaxies were extragalactic. When objects that today we call galaxies were first observed, what clearly distinguished them from stars was their resolved structure. Since this time, structure and morphology has remained one of the most common ways galaxies are described and studied. Initially this involved visual impressions of galaxy forms. This has now been expanded to include quantitative methods to measure galaxy structures all the way back to the earliest galaxies we can currently see.

The first published descriptions of galaxy structure and morphology predate the telescopic era. For example, the Andromeda nebula was described as a "small cloud" by the Persian astronomer Abd al-Rahman al-Sufi in the tenth century (Kepple & Sanner 1998). The study of galaxies remained descriptive until the late twentieth century, although more and more detail was resolved as technology improved. As a result, for about 150 years the science of galaxies was necessarily restricted to cataloging and general descriptions of structure, with notable achievements by Messier and William and John Herschel, who located galaxies or "nebula" by their resolved structure as seen by eye. Even before photography revolutionized the study of galaxies some observers, such as William Parsons, the third Earl of Rosse, noted that the nebulae have a spiral morphology and first used this term to describe galaxies, most notably and famously in the case of M51.

It was, however, the advent of photography that allowed astronomers to study in earnest the morphologies and structures of external galaxies. The most notable early schemes were developed by Wolf (1908) and Lundmark (1926), among others. This ultimately led to what is today called the Hubble classification, which was published in essentially its modern form by Hubble (1926), with the final "Hubble Tuning Fork" established by Hubble (1936) and Sandage (1961). The basic Hubble sequence (**Figure 1**) consists of two main types of galaxies, ellipticals and spirals, with a further division of spirals into those with bars and those without bars. Hubble, and the astronomers who followed him, could classify most nearby bright galaxies in terms of this system.

The development of morphological classification methods continued into the twentieth century, with newer methodologies based solely on visual impressions. For example, de Vaucouleurs (1959) developed a revised version of the Hubble sequence, which included criteria such as bars, rings, and other internal features that were prominent on photographic plates of galaxies. Likewise, van den Bergh (1960, 1976), and later Elmegreen & Elmegreen (1987) developed a system to classify galaxies based on the form of spiral arms and the apparent clumpiness of the light in these arms.
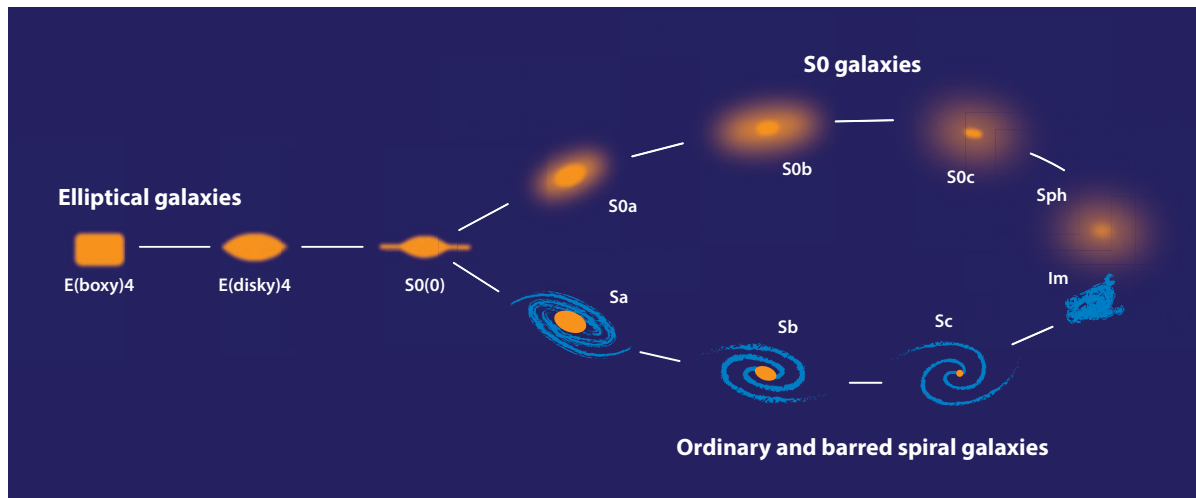
Figure 1

A modern form of the Hubble sequence showing the sequence of ellipticals and S0s and the "tuning fork" in spirals. The elliptical sequence is determined by the overall shape of the galaxy, whereas spiral classifications are divided into different types (a–c), depending on how wound-up the spiral arms are, how large the bulge relative to the disk is, and how smooth the spiral arms in the spirals arm are. The tuning fork is the differential between spirals with and without bars. Also shown is the extension of this sequence to dwarf spheroidal galaxies and irregular galaxies, both of which are lower-mass systems. (Reprinted from Kormendy & Bender 2012 with permission).

Although it is important to classify galaxies visually, and all classification systems have some use, as all features should be explained by physics, it is not obvious which structural features of galaxies are fundamental to their formation history. Ultimately morphology and structure need to be proven useful for understanding galaxies, as there is now extensive use of photometric and spectroscopic methods permitting measurements of perhaps more fundamental measures of stellar populations and dust/gas properties in galaxies. Along these lines, at roughly the same time as when progressively complicated classification systems were developed, astronomers such as Holmberg (1958) established that physical properties of nearby galaxies correlate with morphology in a broad context. Holmberg (1958) found that ellipticals are typically massive and red, and show little star formation, whereas spirals are less massive and bluer and have evidence for ongoing star formation. This quantitatively expands into other physical parameters as well (e.g., Roberts 1963, Roberts & Haynes 1994, Conselice 2006a, Allen et al. 2006). It is also well known that this segregation of morphology in the local Universe provides an important clue for understanding the physics of galaxy formation, especially as local environment is found to strongly correlate with a galaxy's morphology (e.g., Dressler 1984; see Section 4.7).

A revolution in morphological and structurally studies came about with the advent of photometric photometry, and especially the later use of charged coupled devices (CCDs), which made detailed quantitative measurements of light distributions in galaxies possible. The first major contribution from this type of work was by de Vaucouleurs (1948), who used photometry to show that the light profiles of what we would identify today as massive ellipticals all follow roughly the same fundamental light distribution, known as the de Vaucouleurs profile.

This was later expanded by others, most notably Sérsic (1963), who demonstrated that a more general form of light distribution matched galaxy-light profiles with disks having exponential light profiles, whereas the light distribution within massive ellipticals generally follows the

de Vaucouleurs profile. This has led to a large industry in measuring the light profiles of galaxies in the nearby and distant Universe that continues today (Section 2.2).

During the 1970s and 1980s the study of galaxy structure expanded to include the decomposition of galaxy light into bulge and disk profiles (e.g., Kormendy 1977, Caon et al. 1993, Graham & Guzmán 2003) as well as features such as bars, rings, and lenses (e.g., Kormendy 1979, de Vaucouleurs et al. 1991). The three-dimensional structure of disk galaxies was investigated (e.g., van der Kruit & Searle 1982) as well as were detailed studies of bulges and disks in spiral systems (e.g., de Jong 1996, Peletier & Balcells 1996). We also now know there is great diversity in elliptical galaxy internal structures (e.g., Caon et al. 1993, Graham & Guzmán 2003, Kormendy et al. 2009).

Similar investigations demonstrated that secular evolution within disks can provide an explanation for how bars, rings, and lenses can form (e.g., Kormendy 1979, Combes & Sanders 1981). These effects, not driven by hierarchical galaxy formation, are also likely responsible for the formation of pseudobulges and may drive the formation of central massive black holes (e.g., Kormendy & Kennicutt 2004, Sellwood 2013).

Although there is a large amount of work done on the structures and morphologies of galaxies in the nearby Universe (e.g., see Kormendy et al. 2009, Buta 2013, Graham 2013), it is difficult to investigate more than the very basics of structure and morphology when studying distant galaxies. This is owing to the fact that current technology does not allow us to resolve these distant galaxies in the same detail as we can for closer systems. As such, this review concentrates on the features and properties of galaxy structure that we can measure in distant galaxies and how this reveals how galaxy evolution and formation occurs.

The result of this is that one of the areas where galaxy structure and morphology have made their biggest impact is their ability to measure fundamental properties of distant galaxies that we can compare with nearby galaxies to determine evolution. There are extensive methods for studying galaxy evolution such that galaxy structure analyses are becoming an essential aspect of, and providing unique information on, the history and physics of galaxy assembly, which I detail in this review.

1.2. Galaxy Structure within the Context of Galaxy Formation

We know that there is significant evolution in galaxies over time as the stellar mass density of galaxies evolves rapidly at $1 < z < 3$, with about half of all stellar mass formed by $z = 1$ (e.g., Bundy et al. 2005, Mortlock et al. 2011). We also know that there is a vast diversity of star-formation histories for individual galaxies and that the integrated star-formation rate density in the Universe's history peaks at $z \sim 2.5$ and declines at higher and lower redshifts (e.g., Shapley 2011, Madau & Dickinson 2014 in this volume). However, it is not clear from these observations what are/were the driving forces creating galaxies.

Theory offers several approaches for understanding how galaxies form that detailed studies are starting to probe. We now believe that galaxy formation can happen in a number of ways. This includes in situ star formation in a collapsed galaxy, major and minor mergers, and gas accretion from the intergalactic medium. Galaxy structure and morphology are perhaps the best ways to trace these processes, as I discuss in this review.

Another major question I address in this review is how do the structures and morphologies of galaxies change through cosmic time? Major issues that this topic addresses include the formation history of the Hubble Sequence; whether galaxies form "inside-out" or "outside-in"; how long a galaxy retains its morphology; whether morphology is an invariant quantity in a galaxy over a long cosmic time span, and furthermore what relative roles star formation and merging play in galaxy formation.

Galaxy structure and morphology have made a significant impact on these questions largely because of the *Hubble Space Telescope* (HST) and its various Deep Field campaigns starting in the mid-1990s, finding thousands of galaxies at redshifts $z > 1$ within those images. This is complemented by extensive imaging and spectroscopy for nearby galaxies carried out by surveys such as the Sloan Digital Sky Survey (SDSS) and the Millennium Galaxy Catalog (e.g., Shen et al. 2003, De Propris et al. 2007). Combining these surveys makes it possible to study in detail the structures of distant galaxies and to compare these with structures at different redshifts. This has led to a renaissance in the analysis of galaxy structure, including parametric fitting using Sérsic profiles, and the development of nonparametric measurements of galaxy structure that have allowed us to use galaxy morphology/structure as a tool for deciphering how galaxy assembly occurs over cosmic time.

We are in fact now able to resolve galaxies back to redshifts of $z = 8$ with imaging from space and more recently with adaptive optics from the ground (e.g., Akiyama et al. 2008, Conselice & Arnold 2009, Carrasco et al. 2010). This reveals that galaxy structure is significantly different in the early Universe compared with what it is today. It also reveals that there is a progression from galaxies at the highest redshifts—which are small, peculiar, and undergoing high star-formation rates—to the relatively quiescent galaxies that we find in the nearby Universe. How this change occurs, and what it implies for galaxy evolution, is another focus of this review.

Another ultimate goal is to describe the methods for measuring galaxy structure and morphology for nearby galaxies up to the most distant ones we can see. I also discuss how galaxy structure correlates with physical properties of galaxies, such as their star-formation rates, merging, and their overall scale. I then provide a description of the observed structural evolution of galaxies, and a discussion of what this implies for the driving mechanisms behind galaxy formation using the calibrated methods.

The amount of information we have about the structures and properties of galaxies declines as one starts examining higher redshift systems, and issues that arise owing to observational bias must be dealt with. I therefore also discuss systematics that can be addressed through imaging simulations to determine the real evolution of the morphologies and structures of galaxies. I finish this review with a discussion of future uses of galaxy structure/morphology, including the potential with the advent of the *James West Space Telescope* and *Euclid*.

This review is structured as follows. In Section 2, I describe the analysis methods used for measuring the morphologies and structures of galaxies. In Section 3, I describe how structures and morphologies reveal fundamental galaxy properties and evolutionary processes, whereas Section 4 describes the observed evolution of the structures of galaxies through cosmic time. I finish this review with a description of how galaxy structure and evolution are becoming important aspects for understanding the underlying theory of galaxy formation and cosmology in Section 5 and give a summary and future outlook in Section 6.

2. STRUCTURAL MEASUREMENT METHODS

In this section, I describe the various ways in which galaxy structure is measured and quantified for comparisons across all redshifts. There is a great diversity of nearby galaxy properties that cannot be examined at high redshift, and this review only concentrates on general features that can be measured. This includes the traditional approach of using visual estimates to classify galaxies into morphological types as well as quantitative methods. Visual methods have had a resurgence with the advent of Citizen Science projects such as Galaxy Zoo, which provides online tools for nonscientists to classify over a million galaxies (Lintott et al. 2011), as well as large HST projects, such as CANDELS (e.g., Kocevski et al. 2012, Kartaltepe et al. 2014). The bulk of this section,

however, describes the quantitative methods for measuring galaxy structure and the limitations of this approach. The interpretation of what these measurements imply is discussed in Sections 3 and 4.

2.1. Visual Morphology

The classic approach toward understanding the structures of galaxies is through their apparent visual morphology. The major system of classification in use today has developed through Hubble (1926), de Vaucouleurs (1959), and Sandage (1961, 1975), as outlined briefly in the introduction. A modern review of galaxy classification by eye into visual types has been conducted by Buta (2013).

When studying the morphologies of distant galaxies, the visual classifications can only be placed into a few limited and well-defined classes: spirals, ellipticals, and irregulars/peculiars. The spirals can be further subdivided into spirals with or without a bar. In this review, peculiars are interpreted as mergers of two preexisting galaxies, whereas irregulars are lower-mass galaxies that contain a semirandom pattern of star formation, such as that seen in Magellanic irregulars. Typically these irregulars are too faint to be seen at high redshifts and therefore are not considered in this review in any detail.

Visual morphological classifications have been performed on nearly all deep HST imaging starting from its earliest days (e.g., Dressler et al. 1994, van den Bergh et al. 1996). This has continued with deeper and deeper HST observations, including those that sample the rest-frame optical in the near-IR (e.g., Lee et al. 2013, Mortlock et al. 2013). There are, however, some limitations to how these classifications can be used at higher redshifts, as it is not clear how the apparent morphology of a galaxy changes under the influence of redshift effects as opposed to real evolution (Section 2.3.5).

There is also the issue that distant galaxies that look "elliptical" or "disky" do not have the same characteristics as systems with the same morphologies seen nearby (Section 4.1); clearly their properties are different. Features such as sizes, light profiles, colors, and star-formation rates differ within the same galaxy morphological type through time (e.g., Conselice et al. 2011a, Mortlock et al. 2013, Buitrago et al. 2014). Therefore, throughout this review a morphological type is only a visual determination of how a galaxy looks and does not predispose a system to a certain local-galaxy type or template or ascribe a certain formation history or scale.

2.2. Parametric Measurements of Structure

Historically, one of the first ways in which galaxy structure was quantified was through the use of integrated light profiles. These profiles are measured by taking the average intensity of a galaxy at a given radius and then determining how this intensity changes as a function of radius. This was first described in detail by de Vaucouleurs (1948), who used the measurements of light for ellipticals from photometry at different apertures and proposed a fitting form. A similar but more general form was found to better explain the surface brightness profiles by Sérsic (1963) for different types of galaxies,

$$I(R) = I_0 \times \exp\{-b(n) \times [(R/R_e)^{1/n} - 1]\}, \tag{1}$$

where the shape of the profile is described by the Sérsic index, n, and the value of $b(n)$ is determined such that R_e is the effective radius, containing half of the light within the galaxy and is a function of the index n. The standard canonical benchmarks are that the de Vaucouleurs profile is given by $n = 4$ and exponential disks by $n = 1$. In principle, the values of n and R_e are used as fundamental and first-order structural parameters of galaxies.

The use of the Sérsic profile to describe nearby galaxies is extensive (e.g., Caon et al. 1993, Graham & Guzmán 2003, Ferrarese & Jordán 2006, Kormendy et al. 2009, Graham 2013), and it has more recently been applied to distant galaxies, as I discuss in Section 4.2. For reviews on the use of resolved photometry through surface brightness profiles to study early-type galaxies, see e.g., Kormendy & Djorgovski (1989), Allen et al. (2006), and Simard et al. (2011).

Recently the fitting of galaxy two-dimensional profiles with various forms, such as the Sérsic, exponential, and de Vaucouleurs profiles, is done through the GALFIT code by Peng et al. (2002) as well as GIM2D by Simard et al. (2011). These are simple and quick methods for measuring the light profiles and radii of many galaxies, providing data for understanding the evolution of galaxy structure. This allows for the measurements of different light components at high z, although these codes and other similar ones have limitations, such as a constant ellipticity assumption within a given component, but are sufficient for gross measures of galaxy structure.

## 2.3. Nonparametric Measurements of Structure

Another more recent measurement technique involves the nonparametric method of measuring galaxy light distributions. Nonparametric methods of measuring galaxy structure began in the photographic era with attempts to quantify the light concentration in galaxies by Morgan (1962), although extensive quantitative measures were not done until the mid-1990s.

The development of methods to measure the light structures of galaxies began in earnest when the first deep images of distant galaxies were obtained with HST (Schade et al. 1995, Abraham et al. 1996), although their use for low-redshift measurements was also noted at about the same time, but in terms of a physical property rather than a descriptive quantity (e.g., Rix & Zaritsky 1995; Conselice 1997; Bershady et al. 2000; Conselice et al. 2000a,b). These early papers show that quantitative galaxy structure correlates with other parameters, such as color and peculiar features indicating mergers or galaxy interactions (e.g., Rix & Zaritsky 1995, Conselice 1997, Conselice et al. 2000a).

At present, the most common methods for measuring galaxy structure in a nonparametric way is through the concentration (C), asymmetry (A), clumpiness (S) (CAS) system (e.g., Conselice 2003; Sections 2.3.1–2.3.3) and through similar parameters (Takamiya 1999; Papovich et al. 2003, 2005; Abraham et al. 2003; Lotz et al. 2004; Law et al. 2007; Scarlata et al. 2007, Freeman et al. 2013). These parameters are designed to capture the major features of the underlying structures of these galaxies, but in a way that does not involve assumptions about the underlying form, as is done with Sérsic fitting (Section 2.2). These nonparametric parameters are also measurable out to high redshifts, making them ideal for deriving galaxy evolution over many epochs, as we discuss in Section 4.

I give a brief description for how these parameters are measured. Typically, as I discuss below, corrections must be applied to account for noise, and a reproducible radius must be used (e.g., Bershady et al. 2000, Conselice et al. 2000a). This radius issue has been addressed in detail by, e.g., Conselice et al. (2000a), Bershady et al. (2000), and Graham et al. (2005). The radius typically used in these measurements is the Petrosian radius, which is defined as the location where the ratio of surface brightness at a radius, $I(R)$, divided by the surface brightness within the radius, $<I(<R)>$, reaches some value, which is denoted by $\eta(R)$ (Petrosian 1976). The value of η changes from $\eta(0) = 1$, at the center of a galaxy, down to $\eta(\infty) = 0$, when the light from the galaxy is zero at its outer "edge."

This method of measuring the radius is much less influenced by surface brightness dimming than other methods, such as using an isophotal radius, and is therefore useful for measuring the
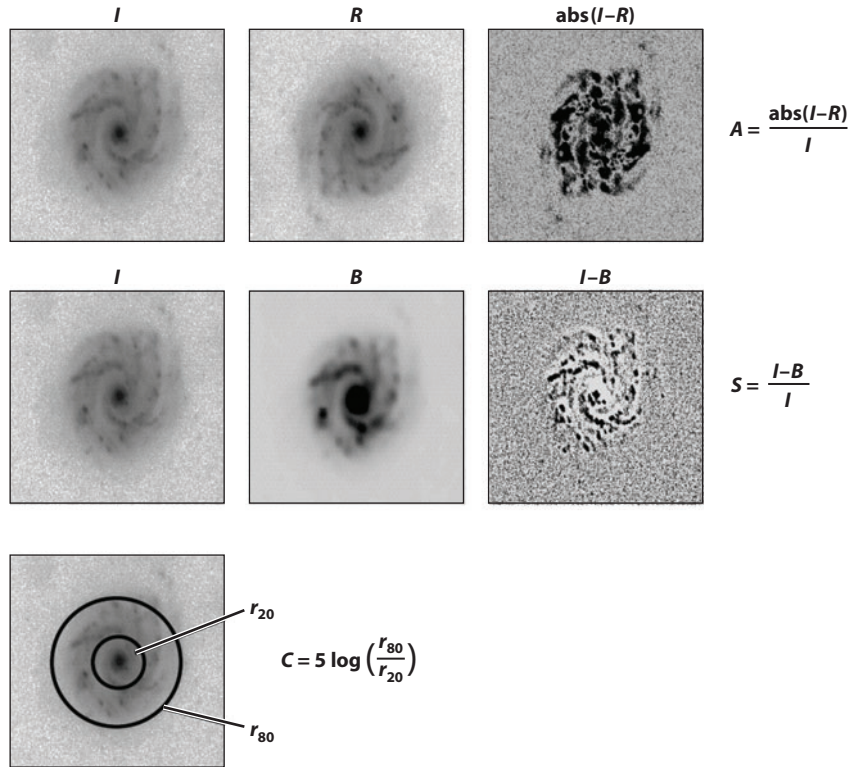
Figure 2

A graphical representation of how the concentration (C), asymmetry (A), and clumpiness (S) are measured on an example nearby galaxy. Within the measurements for A and S, the value "I" represents the original galaxy image, whereas "R" is this image rotated by 180°. For the clumpiness S, "B" is the image after it has been smoothed (blurred) by the factor $0.3 \times 1.5r (\eta = 0.2)$. The details of these measurements can be found in Conselice et al. (2000a) for asymmetry, A, Bershady et al. (2000) for concentration, C, and Conselice (2003) for clumpiness, S.

same physical parts of galaxies at different redshifts (e.g., Petrosian 1976, Bershady et al. 2000, Graham et al. 2005). The mathematical form for this radius is given by

$$\eta(R) = \frac{I(R)}{<I(<R)>}, \tag{2}$$

where most observables in nonparametric morphologies are measured at a radius that corresponds to the location where $\eta(R) = 0.2$ or a relatively small multiplicative factor of this radius (often 1.5 times) (e.g., Bershady et al. 2000, Conselice 2003, Lotz et al. 2004).

2.3.1. Asymmetry index. One of the more commonly used indices is the asymmetry index (A), which is a measure of how asymmetric a galaxy is after rotating along the line-of-sight center axis of the galaxy by 180° (**Figure 2**). It can be thought of as an indicator of what fraction of the light in a galaxy is in nonsymmetric components.

The basic formula for calculating the asymmetry index (A) is given by

$$A = \min\left(\frac{\Sigma|I_0 - I_{180}|}{\Sigma|I_0|}\right) - \min\left(\frac{\Sigma|B_0 - B_{180}|}{\Sigma|I_0|}\right), \tag{3}$$

Table 1 The average concentration (C), asymmetry (A), and clumpiness (S) parameters for nearby galaxies as measured in the optical R-band (Conselice 2003)

Galaxy type	Concentration (R)	Asymmetry (R)	Clumpiness (R)
Ellipticals	4.4 ± 0.3	0.02 ± 0.02	0.00 ± 0.04
Early-type disks (Sa–Sb)	3.9 ± 0.5	0.07 ± 0.04	0.08 ± 0.08
Late-type disks (Sc–Sd)	3.1 ± 0.4	0.15 ± 0.06	0.29 ± 0.13
Irregulars	2.9 ± 0.3	0.17 ± 0.10	0.40 ± 0.20
Edge-on disks	3.7 ± 0.6	0.17 ± 0.11	0.45 ± 0.20
ULIRGs	3.5 ± 0.7	0.32 ± 0.19	0.50 ± 0.40
Starbursts	2.7 ± 0.2	0.53 ± 0.22	0.74 ± 0.25
Dwarf ellipticals	2.5 ± 0.3	0.02 ± 0.03	0.00 ± 0.06

Abbreviation: ULIRGs, ultraluminous infrared galaxies.

where I_0 represents the original galaxy image and I_{180} is the image after rotating it from its center by 180°. The measurement of the asymmetry parameter, however, involves several steps beyond this simple measure. This includes carefully dealing with the background noise in the same way as is done on the galaxy itself, by using a blank background area (B_0) and finding the location for the center of rotation. The radius is usually defined as the Petrosian radius at which $\eta(R) = 0.2$, although out at a large radius the measured parameters are remarkably stable.

Operationally, the area B_0 is a blank part of the sky near the galaxy. The center of rotation is not defined a priori but is measured through an iterative process, whereby the value of the asymmetry is calculated at the initial central guess (usually the geometric center or light centroid), and then the asymmetry is calculated around this central guess using some fraction of a pixel difference. This is repeated until a global minimum is found (Conselice et al. 2000a).

Typical asymmetry values for nearby galaxies are discussed by Conselice (2003): Ellipticals have values at $A \sim 0.02 \pm 0.02$; spiral galaxies are found in the range from $A \sim 0.07 - 0.2$; for ultraluminous infrared galaxies (ULIRGs), which are often mergers, the average is $A \sim 0.32 \pm 0.19$; and merging starbursts are at $A \sim 0.53 \pm 0.22$ (Conselice 2003). **Table 1** lists the typical asymmetry and other CAS values (Conselice 2003). Quantitative structural values for the same galaxy can also differ significantly between wavelengths. This is important for measuring these parameters at higher redshifts, where often the rest-frame optical cannot be probed, an issue I discuss in more detail in Section 2.3.5.

2.3.2. Light concentration. The concentration of light quantifies how much light is in the center of a galaxy as opposed to its outer parts. It is a very simple index in this regard, and it is similar to, and correlates strongly with, Sérsic n values, which are also a measure of the light concentration in a galaxy. There are many ways of measuring the concentration, including taking ratios of radii that contain a certain fraction of light as well as measuring the ratio of the amount of light at two given radii (e.g., Bershady et al. 2000, Graham et al. 2005). These radii are often defined by the total amount of light measured within some Petrosian radius, often at the same location as used for measuring the asymmetry index.

The ratio most commonly used is that of two circular radii that contain an inner and outer fraction (20% and 80% or 30% and 70% are the most common) (r_{inner}, r_{outer}) of the total galaxy flux (**Figure 2**),

$$C = 5 \times \log \left(\frac{r_{\mathrm{outer}}}{r_{\mathrm{inner}}} \right). \tag{4}$$

A higher value of C indicates that a larger amount of light in a galaxy is contained within a central region. The concentration index, however, has to be measured very carefully, as different regions and radii used can produce very different values that systematically do not reproduce well when observed under degraded conditions (e.g., Graham et al. 2001a,b; Graham et al. 2005).

2.3.3. Clumpiness. The clumpiness (or smoothness) (S) parameter is used to describe the fraction of light in a galaxy that is contained in clumpy distributions. Clumpy galaxies have a relatively large amount of light at high spatial frequencies, whereas smooth systems, such as elliptical galaxies, contain light at low spatial frequencies. Galaxies that are undergoing star formation tend to have very clumpy structures and, thus, high S values. Clumpiness can be measured in a number of ways; the most common method used, as described by Conselice (2003), is

$$S = 10 \times \left[\left(\frac{\Sigma(I_{x,y} - I_{x,y}^{\sigma})}{\Sigma I_{x,y}} \right) - \left(\frac{\Sigma(B_{x,y} - B_{x,y}^{\sigma})}{\Sigma I_{x,y}} \right) \right], \tag{5}$$

where the original image, $I_{x,y}$, is blurred to produce a secondary image, $I_{x,y}^{\sigma}$ (**Figure 2**). This blurred image is then subtracted from the original image, leaving a residual map containing only high-frequency structures in the galaxy (Conselice 2003). The size of the smoothing kernel σ is determined by the radius of the galaxy, and the value $\sigma = 0.3 \cdot 1.5 \times r(\eta = 0.2)$ gives the best signal for nearby systems (Conselice 2003). Note that the centers of galaxies are removed when this procedure is carried out as they often contain unresolved high spatial frequency light.

Figure 3 shows a diagram for how these three CAS parameters are measured for a typical nearby spiral galaxy. Furthermore, the CAS parameters can be combined together to create a 3D space in which different galaxy types can be classified. For example, **Figure 3** shows the concentration versus asymmetry versus clumpiness diagram, demonstrating how these parameters can be used to determine morphological types of galaxies in the nearby Universe in CAS space.

2.3.4. Other coefficients. Other popular structural measurement systems are the Gini/M_{20} parameters, which are used in a fashion similar to the CAS parameters to find galaxies of broad morphological types, especially galaxies undergoing mergers (e.g., Abraham et al. 2003, Lotz et al. 2004). These parameters measure the relative distribution of light within pixels and do not involve subtraction, as is used for the asymmetry and clumpiness parameters, and therefore in principle may be less sensitive to high levels of background noise (e.g., Lotz et al. 2004).

The Gini coefficient (G) is a statistical tool originally used in economics to determine the distribution of wealth within a population; higher values indicate a very unequal distribution (Gini of 1 means all wealth/light is in one person/pixel), whereas a lower value indicates a more even distribution among the population (Gini of 0 means everyone/every pixel has an equal share). The value of G is defined by the Lorentz curve of the galaxy's light distribution, which does not take into consideration spatial position.

In the calculation of these parameters, each pixel is ordered by its brightness and counted as part of the cumulative distribution (see Lotz et al. 2004, 2008a). A galaxy in this case is considered a system with n pixels, each with a flux f_i, where i ranges from 0 to n. The Gini coefficient is then measured by

$$G = \frac{1}{|\overline{f}| n(n-1)} \sum_{i}^{n} (2i - n - 1)|f_i|, \tag{6}$$

where $\overline{f}$ is the average pixel flux value.

The second-order moment parameter, M_{20}, is similar to the concentration in that it gives a value that indicates whether light is concentrated within an image. However, an M_{20} value denoting a high concentration (a very negative value) does not imply a central concentration as, in
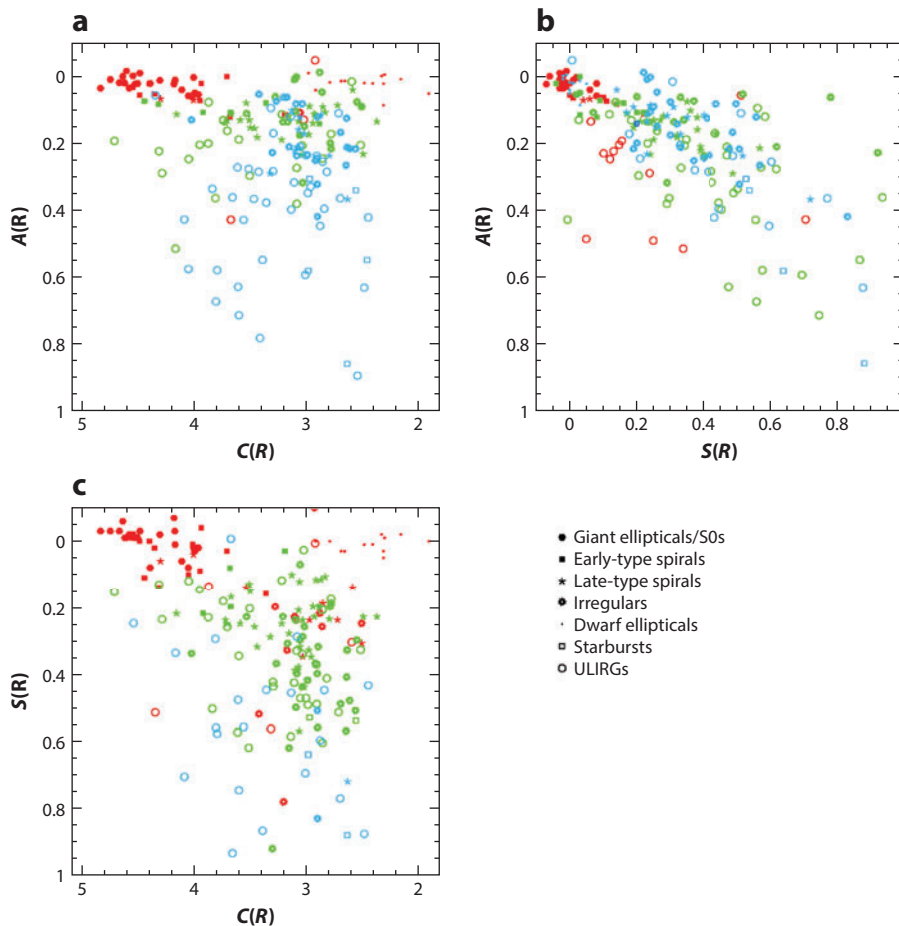
Figure 3

The different forms of the realizations of nearby galaxies of different morphologies and evolutionary states
plotted together in terms of their CAS [concentration (C), asymmetry (A), clumpiness (S)] parameters.
(*a*) The *A-C* indexes are plotted with colored points that reflect the value of the clumpiness for each galaxy.
Systems that have clumpiness values $S < 0.1$ are shown in red, systems where $0.1 < S < 0.35$ are green, and
systems where $S > 0.35$ are blue. (*b*) Similarly, the *A-S* diagram shows concentration values; systems where
$C > 4$ are red, systems where $3 < C < 4$ are green, and systems where $C < 3$ are blue. (*c*) For the *S-C*
diagram, systems having asymmetries $A < 0.1$ are red, systems where $0.1 < A < 0.35$ are green, and systems
where $A > 0.35$ are blue. When using these three morphological parameters, all known nearby galaxy types
can be distinctly separated and distinguished in structural space (Conselice 2003). Abbreviation: ULIRGs,
ultraluminous infrared galaxies.

principle, the light could be concentrated in any location in a galaxy. The value of M_{20} is the mo-
ment of the fluxes of the brightest 20% of light in a galaxy, which is then normalized by the total
light moment for all pixels (Lotz et al. 2004, 2008a). The mathematical form for the M_{20} index is

$$M_{20} = \log 10 \left(\frac{\sum_i M_i}{M_{tot}} \right), \text{ while } \sum_i f_i < 0.2 f_{tot}, \tag{7}$$

where the value of M_{tot} is

$$M_{tot} = \sum_i^n M_i = \sum_i^n f_i \left[(x_i - x_c)^2 + (y_i - y_c)^2 \right];$$

here x_c and y_c indicate the center of the galaxy, and in the case of M_{20} this center is defined as the location where the value of M_{tot} is minimized (Lotz et al. 2004). The separation for nearby ellipticals, spirals, and ULIRGs is similar to that found by the CAS parameters (see Lotz et al. 2004, 2008a).

Other popular parameters include the multiplicity index, Ψ, which is a measure of the potential energy of a light distribution (e.g., Law et al. 2007). Values of Ψ range from 0, for systems that are in the most compact forms, to $\Psi > 10$, which indicates systems that are often very irregular/peculiar (e.g., Law et al. 2012b). Another recent suite of parameters developed by Freeman et al. (2013) includes features that measure the multimode (M), intensity (I), and deviation (D) of a galaxy's light profile with the intention to locate galaxy mergers.

2.3.5. Redshift effects on structure. One of the major issues with nonparametric structural indices is that they change for more distant galaxies, due to not only any evolution but also distance effects, creating a smaller and fainter image of the same system. This must be accounted for when using galaxy structure as a measure of evolution (e.g., Conselice et al. 2000a, Conselice 2003, Lisker 2008).

There are several ways to deal with this issue, and they are similar to how corrections for point-spread functions in parametric fitting or weak lensing analyses are done. The most common correction method for nonparametric parameters is to use image simulations. These simulations are such that nearby galaxies are reduced in resolution and surface brightness to match the redshift at which the galaxy is to be simulated. These new simulated images are then placed into a background appropriate for the instrument and exposure time in which the simulation takes place (Conselice 2003). The outline for how to do these simulations is provided in papers by Giavalisco et al. (1996) and Conselice (2003), among others.

To give some idea of the difficultly in reproducing the morphologies and structures of galaxies, **Figure 4** shows simulated nearby early-type spirals as they would appear in WFC3 imaging data from the Hubble Ultra Deep Field (Conselice et al. 2011a). What can be clearly seen is that it is difficult, and sometimes even impossible, to discern features of these galaxies after they have been simulated.

Another issue when examining the structures of distant galaxies is that these systems are often observed at bluer wavelengths than that typically observed within the nearby Universe owing to the effects of redshift. For example, pictures of galaxies at $z > 1.2$ taken with WFPC2 and ACS are all imaged in the rest-frame UV. **Figure 5** shows what rest-frame wavelength various popular filters probe as a function of redshift. This shows that we must go to the near-IR to probe rest-frame optical light for galaxies at $z > 1$.

It turns out that the qualitative and quantitative morphologies and structures of galaxies can vary significantly between rest-frame UV and rest-frame optical images (e.g., Meurer et al. 1995, Hibbard & Vacca 1997, Windhorst et al. 2002, Taylor-Mager et al. 2007), though these morphologies are not significantly different for starbursting galaxies with little dust at both low and high redshift (Conselice et al. 2000c, Dickinson 2000). Although it is clear that the CAS method works better at distinguishing types at redder wavelengths (e.g., Lanyon-Foster et al. 2012), its use has also expanded into image analyses with H I and dust-emission maps from *Spitzer Space Telescope* (e.g., Bendo et al. 2007; Holwerda et al. 2011, 2012, 2013, 2014).

The process for accounting for the effects of image degradation is to measure the morphological index of interest at $z = 0$ and then to remeasure the same values at higher redshift after simulating.

a   **b**
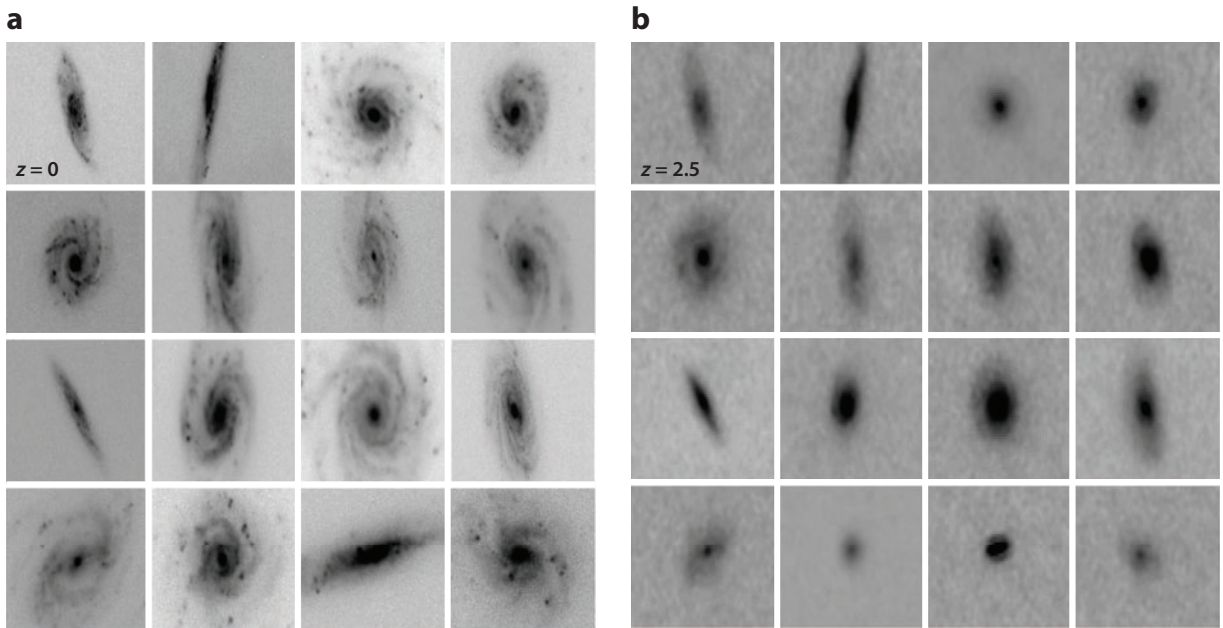
Figure 4

Nearby galaxies (*a*) originally observed at $z = 0$ in the rest-frame B-band (*b*) simulated to show how they would appear at $z = 2.5$, also observed in the rest-frame B-band, within the Hubble Ultra Deep Field WFC3 F160W H-band. These systems are classified as late-type spirals (Sc and Sd) in the nearby Universe, but can appear very different when simulated to higher redshifts as seen here and when using quantitative measures. The galaxies shown here have typical sizes of several kiloparsecs in effective radii and are at a variety of distances (see Conselice et al. 2000a, Conselice et al. 2011a). These changes in structure, both in apparent morphology and in terms of the structural indices, must be carefully considered before evolution is derived (e.g., Conselice et al. 2008, Mortlock et al. 2013).

For the morphological k-correction, the approach has been to measure the parameter of interest at different wavelengths and to determine by interpolation its value at the rest-frame wavelength of interest.

Using the asymmetry index as an example, the final measure after correcting for redshift effects is

$$A_{\text{final}} = (A_{\text{obs}} + \delta A_{\text{SB-dim}} + \delta A_{\text{k-corr}}), \tag{8}$$

where $\delta A_{\text{k-corr}}$ is the (usually negative) morphological k-correction, and $\delta A_{\text{SB-dim}}$ is the (positive) correction for image degradation effects. Other parameters can be measured in the same way. This is a necessary correction to examine the evolution of a selected population at the same effective depth, resolution, and rest-frame wavelength.

3. THE PHYSICAL NATURE OF GALAXY STRUCTURE

The ultimate goals in this review are to trace how structure evolves over cosmic time and to use this as a method to decipher galaxy evolution. In this section I present work to date that describes how physical information is derived from galaxy structural parameters.

3.1. Star Formation and Galaxy Structure

The star-formation process within galaxies is critical, as galaxies do not exist without stars in them. Star formation is also one of the major criteria for classification within the Hubble sequence. The
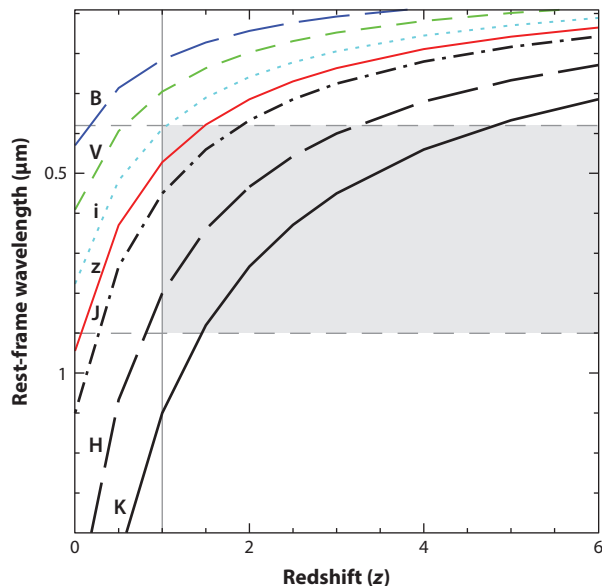
Figure 5

Plot showing the rest-frame wavelength probed by the most common filters used to image distant galaxies as a function of redshift from $z \sim 0$–6. The filters shown are the ACS B_{450}, V_{550}, i_{775}, and z_{950} filters, and the WFC3 J_{110} and H_{160} filters and a K-band filter centered at 2.2 μm. The shaded area shows the region in which the rest-frame optical light of distant galaxies can be probed from between 0.38 μm and 0.9 μm. As can be seen, the H-band allows rest-frame light up to $z \sim 3$ to be imaged, whereas the K-band can extend this out to $z \sim 4.5$.

effects of star formation have also been used to classify spiral galaxies into various classes (e.g., van den Bergh 1976, Elmegreen & Elmegreen 1987).

Star formation is an enormous topic with a great amount of work published (e.g., Kennicutt 1998, Kennicutt & Evans 2012, Madau & Dickinson 2014), and I thus limit my discussion to how star formation and galaxy structure are related. The integrated star-formation density evolution of galaxies in the Universe has been studied in detail and is now well characterized. The integrated star-formation rate increases from a low initial value at $z > 6$ to a peak at $z \sim 2$, and thereafter the rate declines. At higher redshifts $z > 1$, there is also a well-defined relation between star-formation rate and stellar mass, such that higher-mass galaxies have a higher rate of star formation (e.g., Noeske et al. 2007, Bauer et al. 2011).

This is important, as galaxies undergoing star formation can have very different morphologies and structures from passive galaxies. Examples of this include clumpy spiral arms, knots of star formation, central bright starbursts, etc. This can be seen, for example, when viewing local galaxies, whereby those with star formation appear clumpier and more asymmetric than those without star formation.

Furthermore, there are also morphological k-correction effects, such that star-forming galaxies have a smaller difference in their morphology between UV through optical and near-IR light (e.g., Windhorst et al. 2002, Taylor-Mager et al. 2007). This generally reveals that at shorter wavelengths the morphologies and quantitative structures are tracing the distribution of star formation directly. At optical wavelengths longer than the Balmer break, we are sampling a mixture of stars at different ages, with older ages dominating the spectral energy distributions (SEDs) at longer wavelengths. There are also very dusty galaxies such as submillimeter

sources and ULIRGs that can have a significant fraction of their optical light absorbed (e.g., Calzetti et al. 2000).

It is apparently not just morphology that is affected by star formation but also the quantitative structure. It is well known that star-forming galaxies without significant dust are quite blue, but the effects of star formation can also be seen in their structure. Quantitative measurements of structure strongly correlate with the star-formation rate within galaxies as measured by the correlation between the clumpiness index (S) and the Hα equivalent width (Conselice 2003). This is also seen in more asymmetric and clumpy light distributions within Hα imaging of nearby galaxies, and when examining the light distribution at 24-μm imaging using *Spitzer Space Telescope* imaging (e.g., Bendo et al. 2007). Conselice (2003) shows how the clumpiness index can be used as a measure of star formation, and Conselice et al. (2000a) show that asymmetry values correlate strongly with (B-V) color for nearby galaxies.

3.2. Structure as a Merging Indicator

One of the primary physical effects that can be seen in the structures of galaxies is when two galaxies merge or interact with each other. When these dynamical events occur the structures of these systems often become very peculiar and distorted, especially when the merging galaxies contain a similar amount of mass in a major merger. (Note that a major merger throughout this review is a merger in which the ratio of the stellar masses of the progenitors are 1:4 or greater. A minor merger is one with a mass ratio of less than 1:4.) We have learned much about nearby galaxy mergers, such as ULIRGs (e.g., Joseph & Wright 1985, Sanders & Mirabel 1996) through numerical simulations (e.g., Mihos & Hernquist 1996) that have shown convincingly that peculiar galaxies are often mergers (Toomre & Toomre 1972). This demonstrates that there is a strong correlation between structure and this fundamental galaxy formation process.

Early measurements of nearby galaxies found a correlation between galaxy lopsidedness, quantified through Fourier decomposition of structure and the asymmetry parameter, and the presence of interacting or merging neighbors (e.g., Rix & Zaritsky 1995, Conselice 1997, Reichard et al. 2008). As such, galaxy structure is a powerful method for determining whether a galaxy is undergoing a recent major merger. This has been measured in many ways, from using visual estimates of mergers based on peculiar structures to examining more quantitative results.

One automatic method for finding mergers is the CAS approach (Conselice 2003), in which merging galaxies are those with a high asymmetry that is also higher than the value of the clumpiness. The simple condition

$$(A > 0.35) \& (A > S) \tag{9}$$

accounts for a large fraction, but not all, of local galaxies that are mergers—i.e., ULIRGs and starbursts in mergers (see **Figure 3**). Although the contamination from nonmergers is fairly low (at a few percent), the fraction of actual mergers that are identified is roughly 50% (Conselice 2003). This is largely due to the fact that galaxies involved in the merger process are only quantitatively asymmetric for about a third of the lifetime of the merger (see Section 3.4).

There is also the relationship found by Lotz et al. (2008a) for locating major mergers using Gini/M_{20} parameters, which is given by,

$$G > -0.14 \times M_{20} + 0.33. \tag{10}$$

More recent criteria developed by Freeman et al. (2013) use multimode (M), intensity (I), and deviation (D) statistics to quantify which galaxies are mergers. Their study shows that a higher fraction of real mergers can be found using these indices compared with CAS or Gini/M_{20}.

One ultimate result of finding these mergers is that it allows us to calculate the merger fraction within a population of galaxies. The basic merger fraction (f_m) is calculated as the number of mergers selected within a given redshift bin and stellar mass limit (or luminosity cut) (N_m) divided by the total number of galaxies within the same redshift bin and stellar mass selection (N_T). The merger fraction is thus defined as

$$f_m(M_*, z) = \frac{N_m}{N_T}. \tag{11}$$

This merger fraction is also a function of stellar mass and redshift. The CAS mergers are nearly all major mergers (Conselice 2003, 2006b; Lotz et al. 2008b), whereas Gini/M_{20} measure all types of mergers, both minor and major.

Furthermore, for structural samples, we calculate the merger fraction as opposed to the galaxy merger fraction. The difference is important when comparing with pair studies in which the two progenitors can be resolved. The difference between these two is subtle, but important. The merger fraction considers a merger as having already happened; the two galaxies that have merged now count as a single system. The galaxy merger fraction is the fraction calculated when both of these merging galaxies are considered as two separate galaxies, which they were before the final merger.

The galaxy merger fraction (f_{gm}) is thus the number of galaxies merging, where a system that has already condensed into a single galaxy is counted as two galaxies, divided by the number of galaxies in the total sample. For small merger fractions this ratio is about a factor of two larger than the merger fraction that counts only the merger remnants (Conselice 2006b). The equation to derive the galaxy merger fraction with observables through morphology, with the assumption that every merging galaxy has exactly two progenitor galaxies, is given by

$$f_{gm}(M_*, z) = \frac{2 \times N_m}{(N_T + N_m)} = \frac{2 \times f_m}{(1 + f_m)}. \tag{12}$$

This relation does not hold if a merger occurs with more than two galaxies (Conselice 2006b), although these are very rare (de Propris et al. 2007). The morphological measurement of the nearby merger fraction gives values of $f_m = 0.01$ (de Propris et al. 2007). A discussion of the measurement of this at higher redshifts is included in Section 4.3.

3.3. Galaxy-Scale Properties and Galaxy Structure

One of the interesting facts about galaxies is that many of their characteristics can be explained by an underlying property, which is likely the galaxy's halo or total mass (Caon et al. 1993, Disney et al. 2008). As an example, it was noted early on that galaxy light profile shapes of ellipticals correlated strongly with the radius or magnitude of a galaxy (e.g., Caon et al. 1993). This implies that the scale or mass of an elliptical galaxy has an influence on a galaxy's overall light profile and shape.

This can also be seen in the detailed structures of galaxies. In general it appears that on average galaxies with a higher degree of central concentration have larger total or stellar masses. This is also seen in the concentration index, which is another measure of the degree of light concentration; more massive galaxies have a higher value of concentration (e.g., Conselice 2003). This concentration also correlates with the fraction of light in bulge and disk components. This relation is such that the more concentrated a galaxy is, the less likely it contains a significant disk (e.g., Conselice 2003). In fact, it is likely that it is the fraction of bulge light that drives this correlation, and more massive systems are more likely to have significant and concentrated bulges.

Concentration also separates galaxies having different star-formation histories in the local and high-redshift Universe. In a study using the Sloan Digital Sky Survey (SDSS), Strateva (2001)

showed that nonstar-forming galaxies are more concentrated than star-forming blue systems. This can also be demonstrated by other overall galaxy properties (e.g., Allen et al. 2006, Conselice 2006a). The light concentration for ellipticals also correlates with the mass of the central massive black hole (e.g., Graham et al. 2001, Savorgnan et al. 2013).

3.4. Numerical Simulations of Galaxy Structure

Simulations of galaxy formation are critical for interpreting and understanding the meaning of structural indices of galaxies. In fact, one of the first computer simulations of galaxy formation by Toomre & Toomre (1972) showed that the peculiar morphologies of galaxies seen in, e.g., the Arp (1966) atlas were due to systems undergoing major mergers rather than some other cause. Since then, numerical simulations of galaxies have proven an effective method for interpreting the structures and morphologies of galaxies in both the local Universe and at higher redshifts. In many ways this approach toward understanding galaxy morphology has just begun and promises to be a powerful and effective approach for interpreting the meaning of structure in the future.

Mihos & Hernquist (1996) provided one of the first papers to demonstrate in detail how the peculiar galaxies seen in deep HST imaging were in fact due to the merger process using the TREESPH hydrodynamical method from Hernquist & Katz (1989). Interest in comparing simulated merger results with observables was largely in terms of starbursts and SEDs of galaxies (e.g., Barnes & Hernquist 1991). However, some attempts were made even very early to use these merger N-body models as methods of interpreting HST morphologies of galaxies (Mihos 1995).

Applying quantitative structural methods described in Section 2 to these numerical simulations of structural evolution was first carried out by Conselice (2006b), who used the CAS method to calculate the timescale of the merger process on dark-matter particle simulations, finding a merger timescale of $\sim$0.3–0.8 Gyr for galaxies having a high-enough asymmetry to be identified as an unambiguous merger (Section 3.2). This timescale is critical for interpreting galaxy merger fractions through cosmic time, as it allows us to convert merger fractions to merger rates and thus derive how mergers are driving galaxy formation. Using these results, Conselice (2006b) deduces that a typical galaxy undergoes $4.4^{+1.6}_{-0.9}$ mergers from $z \sim 3$ to $z \sim 0$.

Conselice (2006b) also shows that the time when a merger is asymmetric is distributed throughout the merger process and is not located at one particular time. Moreover, the merging systems would not always be identifiable as such when studied with the CAS parameters. In addition to giving a robust timescale, Conselice (2006b) also shows that only a fraction (about a third) of a merging galaxy's time sequence would be identified as a major merger using CAS. The timescale derived is also largely independent of the viewing angle of the merger, and an asymmetry signal is only present within major mergers with mass ratios of 1:4 or greater.

The simulations used by Conselice (2006b) are, however, simple in that they do not include the effects of star formation or dust, which are well known to produce dramatic changes in morphology (e.g., Taylor-Mager et al. 2007; and see Section 2.3.5). When star formation and dust are added to simulations of galaxy structure the quantitative structural parameters measured are similar to those seen in nearby galaxies, and the measured structure correlates with other properties, such as color, in the same way it does for nearby galaxies (e.g., Lotz et al. 2008b, Hambleton et al. 2011).

Lotz et al. (2008b) include the first measurements of CAS and Gini/M_{20} parameters on numerical simulations that include old and young stars, star formation, gas, and dust. Lotz et al. (2008b, 2010a,b) use GADGET/N-body/hydrodynamical simulations of galaxies when imaging the appearance of these galaxy mergers. Lotz et al. (2008b) utilize disk galaxies of the same total mass, whereas later they investigate mergers with a variety of mass ratios (Lotz et al. 2010a) and examine how the amount of cold gas mass in progenitor galaxies influences morphology (Lotz et al. 2010b).
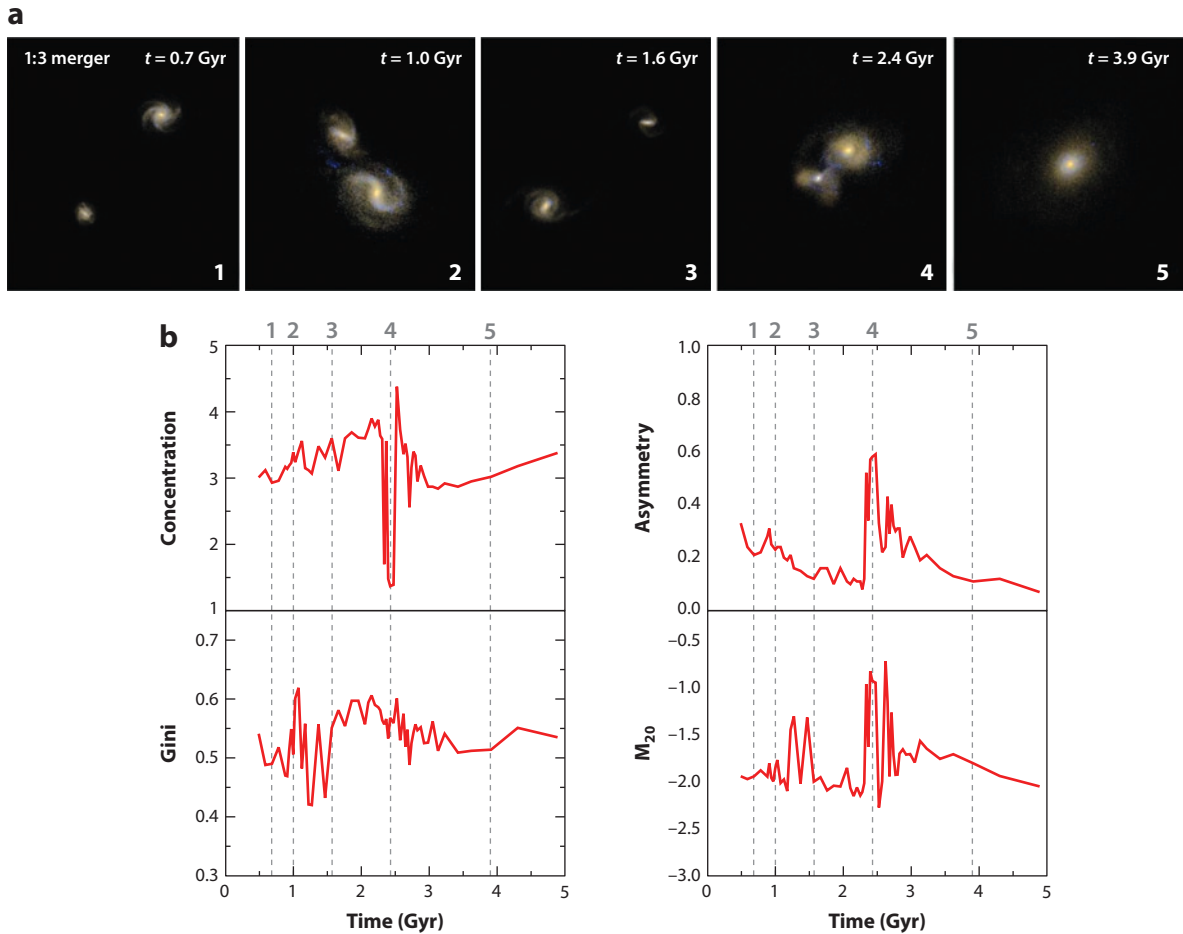
Figure 6

An N-body/hydrodynamical model from Lotz et al. (2008b, 2010a) showing two equal-sized disk galaxies merging as a function of time. (*a*) The numbers across the top of the realizations of this model show the various snapshots of time through the simulation, whereas (*b*) the bottom panels show the changes in the concentration, asymmetry, Gini, and M_{20} values for this particular simulation. This demonstrates the changing form of quantitative indices during a merger and how these systems are only identifiable within the different morphological systems as a merger at specific times. Courtesy of Jennifer Lotz.

These simulation results are passed through the SUNRISE Monte-Carlo radiative transfer code to simulate, as realistically as possible, how galaxies would appear based on the simulation output.

Lotz et al. (2008b, 2010a,b) further investigate the location in CAS and Gini/M_{20} parameter space for mergers in different scenarios and for different properties of the merging galaxies. They investigate the timescale for how long these simulated galaxies appear as a "merger" on the basis of where they fall in these nonparametric structural spaces (see **Figure 6** for an example of these simulations). These papers also investigate how the dust, viewing angle, orbital parameters, gas properties, supernova feedback, and total mass alter the structural merger timescale. Lotz et al. (2008b, 2010a) find that most properties—the total mass, supernova feedback, viewing angle, and orbital properties of mergers—have very little influence on the derived timescales. The mass ratio and gas mass fraction of the merging galaxies affect the derived merger timescales significantly, however.

Mergers are identified within both CAS and Gini/M_{20} at the first pass of the merger as well as when the systems finally coalesce to form a remnant (Lotz et al. 2008b). However, merging galaxies are not found in the merger area of the nonparametric structural parameters for the entire merger. This, however, allows the timescales for structural mergers to be calculated. Lotz et al. (2008b, 2010a) find that the asymmetry timescales for gas-rich major mergers are 0.2–0.4 Gyr and 0.06 Gyr for minor mergers (Lotz et al. 2010a). The Gini/M_{20} timescales are $\tau_m = 0.2 - 0.4$ Gyr. These are relatively quick timescales and, thus, suggest that the observed merger fraction converts to a high merger rate.

This is similar to, but not exactly the same as, the dynamical friction merger timescales calculated for merging objects that have a separation change from r_i to r_f. The dynamical friction timescale is given by t_{fric}:

$$t_{fric} = 0.0014 \, \text{Gyr} \, (r_i^2 - r_f^2) \left(\frac{v_c}{100 \, \text{km} \, \text{s}^{-1}} \right) \left(\frac{10^{10} \, \text{M}_\odot}{M} \right), \tag{13}$$

where v_c is the relative velocity between the two merging galaxies at a given time, M is the mean accreted mass, and the Coulomb logarithm $\ln \Lambda = 2$ (Dubinski et al. 1999). Dynamical friction calculations such as these have dominated the calculation of galaxy timescales up until simulations of mergers revealed more subtle results, although the blunt calculations from Equation 13 are often a good rough estimate for merger timescales, giving values of ∼0.5 Gyr for equal-mass mergers.

Lotz et al. (2008b, 2010a) also find that the asymmetry index is sensitive to major mergers of ratios of 1:4 or less, whereas the Gini/M_{20} parameters are sensitive for mergers down to 1:9, which enables probing more minor mergers. Lotz et al. (2010b), however, find that very gas-rich galaxies, such as those seen in high redshift, may have longer timescales for merging with gas-rich progenitors, which are likely to be more common at higher redshifts. This would provide a "merger" asymmetry signal for more minor mergers as long as they were more gas rich. However, it is clear that massive galaxies with $M_0 > 10^{10} \, \text{M}_\odot$, where most measurements have been made to date at $z < 3$, have a low gas mass fraction (e.g., Erb et al. 2006, Mannuci et al. 2010, Conselice et al. 2013).

4. MEASUREMENTS OF GALAXY STRUCTURAL EVOLUTION

The above sections describe how we can measure the structures and morphologies of galaxies through various approaches as well as the meaning of these structures and morphologies. In this section, I discuss how these measurements have been applied to galaxies at all redshifts to decipher how evolution is occurring within the galaxy population.

When galaxies were first found in the distant Universe, they were not resolved enough to study their structures and morphologies, and the evolution of galaxies was observationally driven by number counting and colors (e.g., Koo & Kron 1992), and the "faint blue galaxy excess" problem at faint magnitudes dominated the field for twenty years until redshifts for these systems became available (e.g., Ellis 1997).

The problem of galaxy evolution and formation is a large one, and this review does not focus on this question, although I give a brief overview here of the important questions in understanding galaxy evolution. I also demonstrate where galaxy structure and morphology reveal information that cannot be provided by other methods. For a general review of galaxy properties at $z > 2$ see Shapley (2011) for an observational perspective and Silk & Mamon (2012) for a theoretical one. For nearby galaxies a few recent relevant reviews have been provided by Blanton & Moustakas (2009), van der Kruit & Freeman (2011), and Conroy (2013).

Galaxies are now studied up to redshifts of $z \sim 7$–10, although at the highest redshifts less information is available. The most common measures for these distant galaxies are colors, stellar masses, star-formation rates, sizes, and basic structures. From these we know that the volume integrated star-formation rate increases with time from these ultrahigh redshifts until around $z \sim 2$, when the star-formation rate begins to decline (see Madau & Dickinson 2014 in this volume). Stellar mass measurements roughly agree with this picture, such that about half of all stellar mass is formed by $z \sim 1$ (e.g., Mortlock et al. 2011). Galaxies are also much bluer in the past (Finkelstein et al. 2012), and there is some debate and uncertainty concerning the star-formation history of individual galaxies and the relevant role and commonality of very old and/or very dusty galaxies at redshifts $z > 1$.

What is largely unavailable from examining stellar masses, stellar populations, and star-formation histories is how these galaxies assembled. Clearly galaxies are fed gas or have very large gas reservoirs in them to sustain and produce star formation. How this gas gets into galaxies is a fundamental question, as is the relative role of mergers versus star formation in forming galaxies. Because the number of massive galaxies at high redshifts is a factor of ten or so less than those in existence today, clearly much evolution and formation in these systems has occurred.

Galaxy structure provides a way to examine this problem, as it permits us to determine which modes of galaxy formation are active within a galaxy. The first and by far the most common method is to study the merger history through the techniques described in Section 3.2. Another method is to simply examine the visual morphologies of galaxies to determine when the Hubble sequence is in place and combine those results with color, size, and star-formation rates to determine when spirals and ellipticals are roughly in their current form. In particular, the examination of the sizes of galaxies has provided an evolutionary puzzle, such that galaxies of similar masses are up to a factor of 2–5 times smaller than corresponding galaxies seen today (e.g., Buitrago et al. 2008, Cassata et al. 2013).

Furthermore, resolved imaging allows us to study the formation history of individual components of galaxies, such as disks, bulges, spiral arms, clumps of star formation, etc., which reveals formation information not available when examining the galaxy as a whole. This section, which is the heart of this review, provides the current observational evidence for morphological and structural evolution and what it implies for galaxy formation.

4.1. Observed Evolution of the Hubble Sequence

This section of the review examines the formation and evolution of the Hubble sequence. I discuss here only observations that answer the question of when galaxy types appear, without addressing the "how" of their formation mechanisms, which is discussed later in this review. I first describe the bulk morphological evolution in Section 4.1.1, which includes when Hubble types (spirals and ellipticals), as well as peculiar galaxies, formed. I then discuss in the next subsection (Section 4.1.2) the evolution and formation of the more detailed aspects in the Hubble sequence. Specifically I address observations of the earliest observed spiral arms, how the bar fraction in spirals evolves, and how the relative properties of bulges and disks change through time.

4.1.1. Bulk morphological evolution.
The first science result I discuss is how the visual Hubble sequence evolves throughout the Universe. This can simply be restated as measuring the number density and relative fractions of galaxy types at a given selection, which are classified as ellipticals, spirals, and peculiars. As mentioned earlier, I do not consider irregulars as these are typically lower-mass galaxies that are not detected at high redshift owing to their faintness. It is also largely impossible to use finer classifications, such as Sa or Sb, on distant galaxies, as the resolution is

not good enough, even with HST imaging, to resolve this type of detail. More distant galaxies also appear to be quite different from Hubble types, making these types of detailed morphologies unnecessary and undesirable (e.g., Conselice et al. 2005).

This relates to a fundamental question that has been asked since galaxies were discovered, which is whether or not a galaxy retains its morphology over a long period of cosmic time. Otherwise, if morphological transformations do occur, what processes drive this (internal or external), and how often does a galaxy change its morphology?

One of the first observations noted when examining the first deep HST images was that many of the fainter galaxies were peculiar (e.g., Driver et al. 1995, Glazebrook et al. 1995, Schade et al. 1995, Abraham et al. 1996). These early studies were limited to examining galaxy number counts, as no redshifts were known for these faint galaxies. In addition to a faint blue excess, it was clear that there was also a peculiar excess, often for the faintest galaxies. This is where the field remained until redshifts for a significant number of these peculiar galaxies were obtained.

The field of high-redshift studies changed dramatically in 1995–1997 with the advent of the Hubble Deep Fields (HDFs) (Williams et al. 1996, Ferguson et al. 2000) and the discovery of a significant population of high-redshift galaxies that could be discovered by the Lyman-Break technique (Steidel et al. 1996, Shapley 2011), now referred to as Lyman-Break Galaxies (LBGs). The HDFs, and later significant campaigns to obtain very deep Hubble imaging, such as the Hubble Deep Field South (Williams et al. 2000), the Great Observatories Origins Deep Survey (GOODS) (Giavalisco et al. 2004), the Hubble Ultra Deep Field (UDF) (Beckwith et al. 2006), the COSMOS field (Scoville et al. 2007), the Extended Groth Strip survey (EGS) (Davis et al. 2007), and most recently the CANDELS survey (Grogin et al. 2011, Koekemoer et al. 2011), have revolutionized the field of galaxy-formation studies and in particular the study of morphologies.

The critical nature of these deep fields is not simply that they are deeper than previous deep HST imaging but that they are the fulcrum of large-scale efforts to obtain photometry at the faintest levels possible at nearly all wavelengths. This allows redshifts to be measured for most galaxies using photometry through so-called photometric redshifts [e.g., Dahlen et al. (2013) for a recent discussion of the use of this method]. The availability of these redshifts allows us to measure evolution over broad redshift ranges that were not possible before, as spectroscopic samples were few and far between, even with the use of relatively large multislit spectrographs, such as LRIS on Keck (e.g., Cohen et al. 1996).

Early observations using a mixture of spectroscopic and photometric redshifts showed that the Hubble sequence was certainly not in place at high redshifts $z > 1$ (van den Bergh et al. 1996) when examined using WFC2 data. This was verified in the rest-frame optical after deep near-IR NICMOS observations of the HDF were taken in 1998 (Dickinson 2000). A deeper analysis showed that, using the rest-frame optical structures of galaxies, the Hubble sequence was nearly completely absent at $z > 2$, and only at $z \sim 1.5$ did spirals and ellipticals become as common as peculiar galaxies (Ravindranath et al. 2004, Conselice et al. 2005, Buitrago et al. 2013; **Figure 7**).

The latest results on the evolution of visual morphology, as defined solely by visual types, from the CANDELS survey, is shown in **Figure 8** (Mortlock et al. 2013) for systems with stellar masses $M_* > 10^{10} M_\odot$. It must be stressed that this figure only shows the visual esti-mates of galaxy morphology. The classification of a spiral, elliptical, or peculiar does not im-ply that these galaxies have a certain star-formation rate, color, mass, or size. In fact what is often seen is that these visual morphologies do not correlate well with other physical prop-erties (e.g., Conselice et al. 2011b, Mortlock et al. 2013). What is also seen is a stellar mass difference in the formation history of the Hubble sequence, with the highest-mass galaxies appearing to form into visual ellipticals and disks before lower-mass systems (Mortlock et al. 2013).
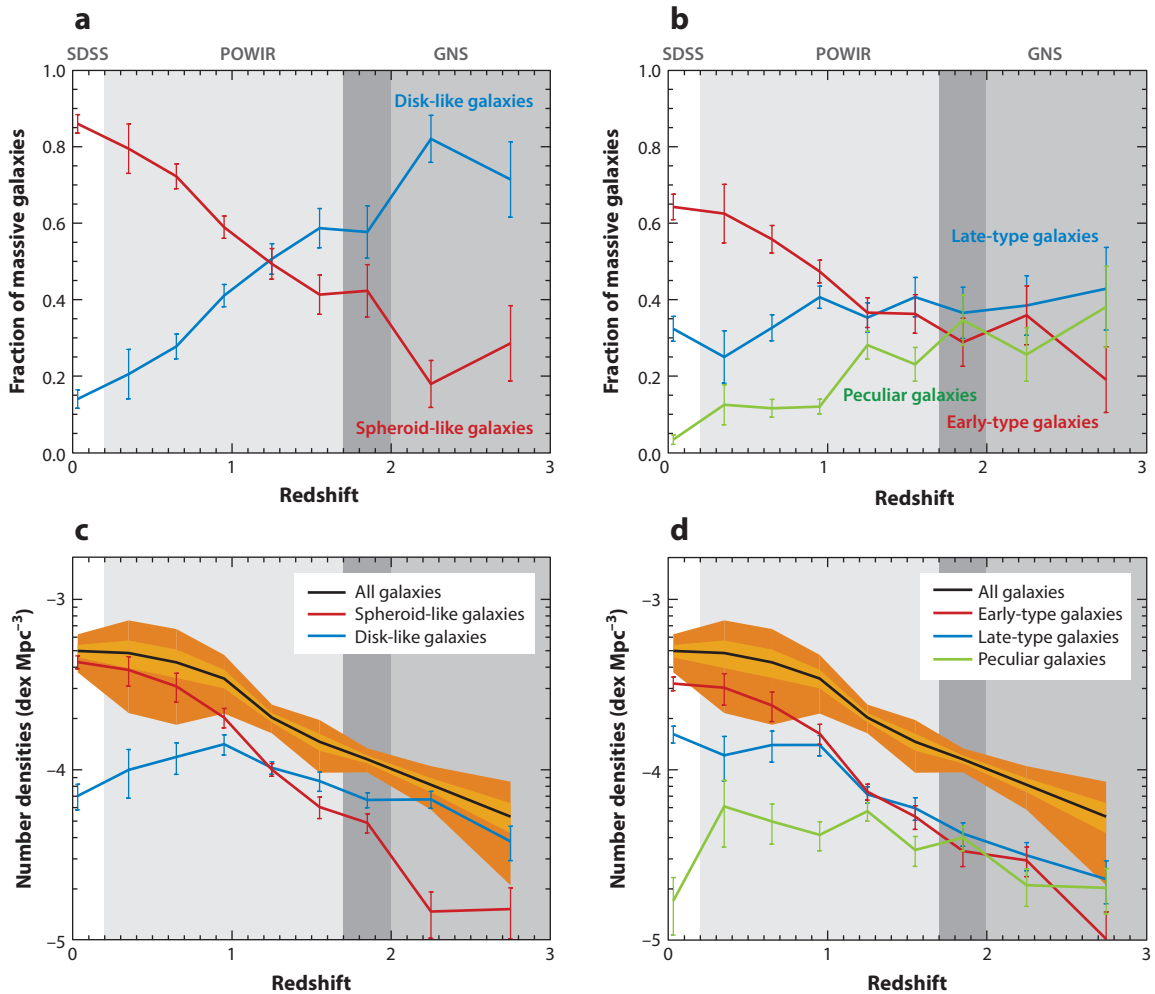
Figure 7

The evolution of apparent morphology and Sérsic-index-based classifications for massive galaxies with $M_* > 10^{11} M_\odot$ from Buitrago et al. (2013). Shown are the morphologies and structures derived from three different surveys—the Sloan Digital Sky Survey (SDSS) for nearby galaxies, the POWIR survey (Conselice et al. 2007) for systems up to $z \sim 2$, and the Great Observatories Origins Deep Survey NICMOS survey (GNS) for systems at $z \sim 1.8-3$. (*a*) In this plot, disk-like galaxies are those with Sérsic indices $n < 2.5$, and spheroid-like galaxies are for those with $n > 2.5$. (*b*) The morphological evolution as judged from visual estimates. Plotted here are both the fraction of types and the number density evolution. (*c,d*) The orange shading gives the total number density of all galaxies as a function of redshift up to $z \sim 3$. As can be seen, there is a gradual transition from galaxies that appear peculiar and "disk-like" in their Sérsic indices at high redshifts $z > 1.5$, which gradually transform into early types today.

What **Figures 7** and **8** show is that at $z > 2$ the dominant morphological type is peculiar, whereas disks and ellipticals become more common at lower redshifts (see also Conselice et al. 2005, Kriek et al. 2009, Delgado-Serrano et al. 2010, Mortlock et al. 2013). **Figures 9** and **10** show images of the most massive galaxies at both $z < 1$ and $z > 2$ in the Hubble UDF, demonstrating the stark differences between the two. This review later examines in Section 4.3 what these peculiars are potentially evolving into at lower redshifts. There is, however, a general trend such that peculiar systems and galaxies with internal features, such as blobs, have a higher star-formation rate than
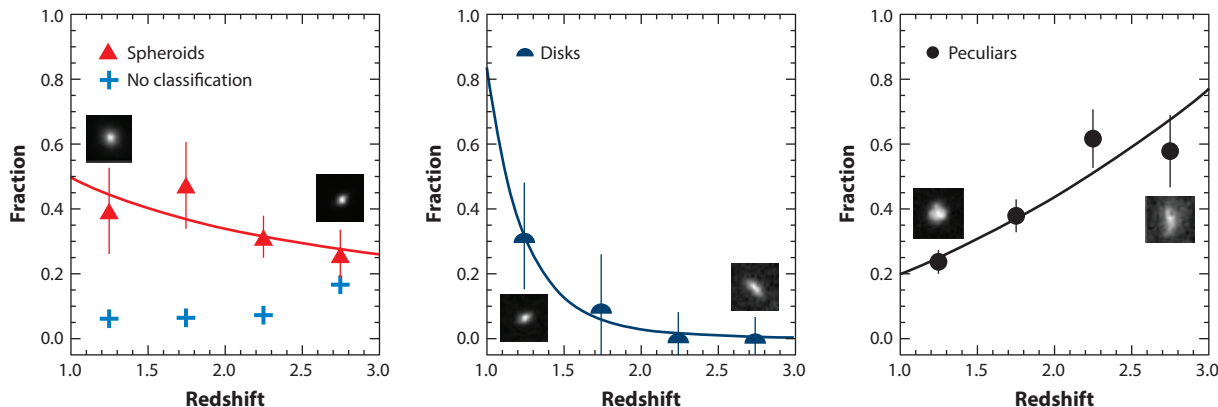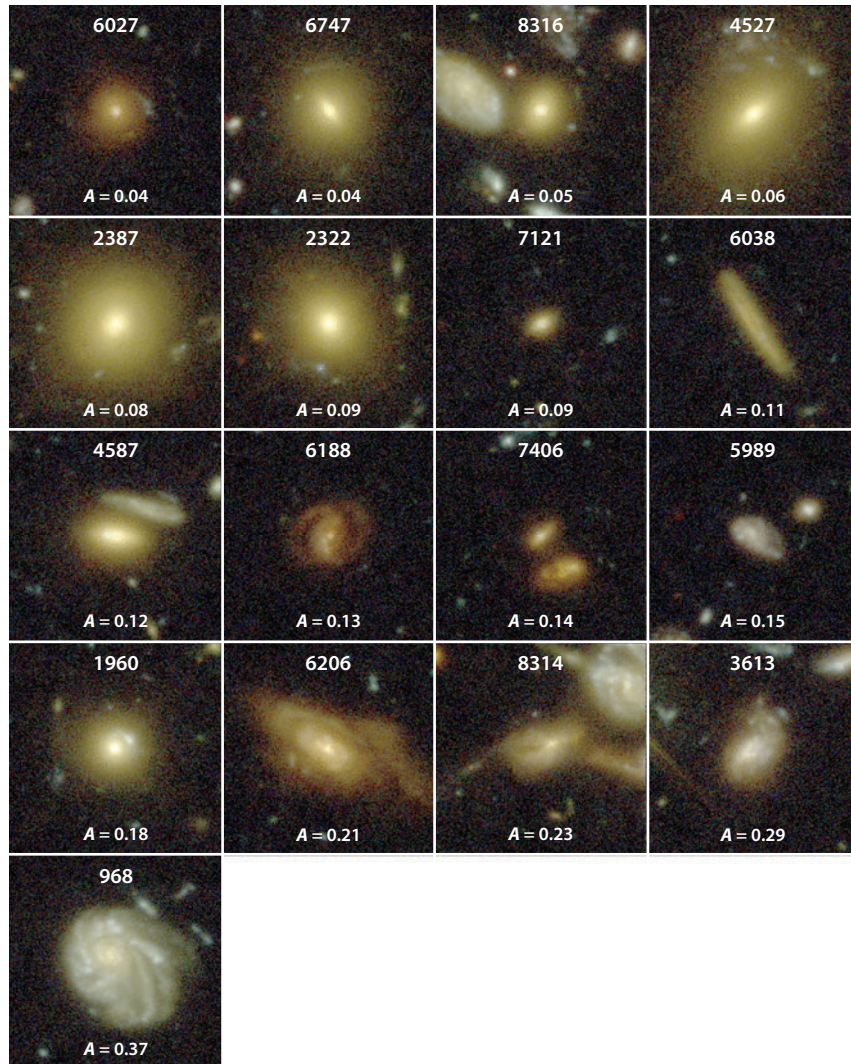
Figure 8

The latest version of the evolution of the Hubble sequence with redshift for galaxies with $M_* > 10^{10}\,M_\odot$. These classifications are corrected for image degradation such that misclassifications owing to distance are accounted for within these fractions (Mortlock et al. 2013). Examples of images of galaxies in each of these bins are shown in the observed H_{160}-band or rest-frame optical. Further analysis shows that there is a downsizing trend such that the most massive galaxies form into Hubble sequence galaxies earlier than lower-mass galaxies (Mortlock et al. 2013).

smoother galaxies (e.g., Lee et al. 2013). This shows that though the Hubble sequence itself is not formed early in the history of the Universe, there are trends that suggest it is becoming established.

Another interesting aspect to examine is not only the fraction of different galaxy types at various redshifts but also their number density evolution as a function of galaxy type. We know from galaxy stellar mass measurements that the most massive systems are largely in place at $z \sim 1$ at the same number density as at $z \sim 1$ (e.g., Bundy et al. 2005, Mortlock et al. 2011). It is the lower-mass galaxies that typically increase the most in terms of the relative number density from the epoch $z \sim 0$–2. In the nearby Universe most of the massive galaxies are ellipticals; this implies that most of the evolution in morphology is also within the lower-mass galaxies, which is what is found. In addition to a mass downsizing, we also find a morphological downsizing, such that morphological ellipticals are formed before the other galaxy types, most notably the spirals. However, whether these galaxies are inherently similar to the ellipticals and disks today is a separate question.

4.1.2. The formation of ellipticals and disks: bars, bulges, disks, and spiral arms. One of the major questions in galaxy evolution we would like to address is when modern spirals and ellipticals form. This is related to the formation of the Hubble sequence, but requires a more detailed answer because what appears as an elliptical/spiral may be quite different from systems classified this way in the local Universe. We thus are interested in determining when systems with the same morphology as galaxies we see in the local Universe (i.e., disks and ellipticals) achieve a similar physical state as measured through other properties. Although morphological fractions are similar at $z \sim 0.5$–0.8, as seen in the nearby Universe, similar physical properties of galaxies—such as colors, star-forming knots, and tidal features—have not reached the same level as locally. It is only recently at $z < 0.3$ that the galaxy population appears in most ways similar to that of today. This question can also be further divided into many subquestions, but for the purpose of this review, I examine the formation history of galaxies identifiable as disks and ellipticals in their gross morphology as well as the formation of more detailed features such as spiral arms, bulges, and bars.

One major issue is the bar fraction of galaxies and how it has evolved with time. Early studies found that the bar fraction evolves significantly (Abraham et al. 1999b), whereas later studies found
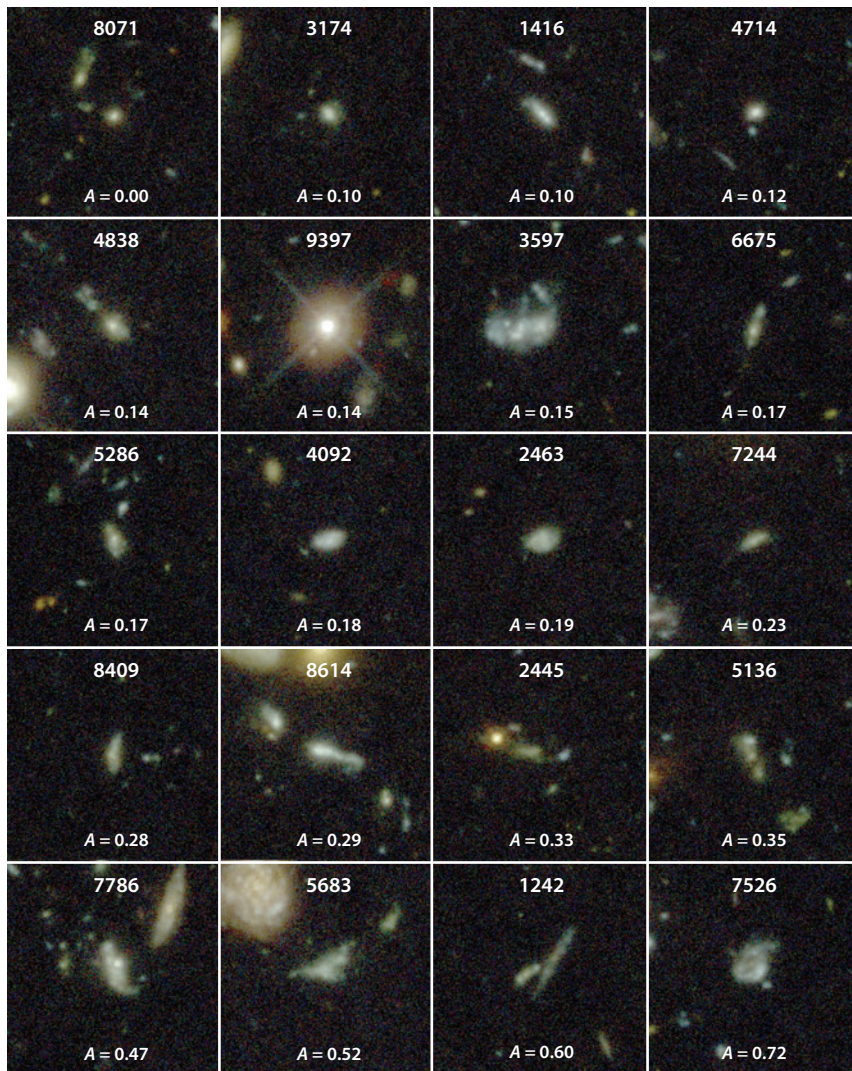
Figure 9

Galaxies in the Hubble Ultra Deep Field as imaged through the ACS camera and ordered by how asymmetric they are. These are all galaxies with redshifts $0.5 < z < 1.2$ and stellar masses $M_* > 10^{10}\,M_\odot$. The ID is the number used by Conselice et al. (2008), and the A value is the value of the asymmetry. At these redshifts most of the massive galaxies can still be classified as being on the Hubble sequence.

that bars were already in place up to $z \sim 1$ (Elmegreen et al. 2004, Jogee et al. 2004). Using the two-degree area COSMOS HST survey, Sheth et al. (2008) find that the bar fraction increases from $z = 0.84$ to $z = 0.2$, from 20% to $\sim$60% of all disk galaxies. Sheth et al. (2008), however, find that the bar fraction is roughly constant with redshift for the most massive and red disk galaxies. In fact most of the observed evolution occurs for the lower-mass bluer disk galaxies.

The fraction of spiral galaxies with bars tells us when the disks in these galaxies become dynamically mature enough to form these structures. The fraction of bars also allows us to determine whether bars have a role in the evolution of star formation and bulge formation and in

Figure 10

Massive galaxies in the Hubble Ultra Deep Field as imaged through the ACS camera and ordered by the value of their asymmetries from most symmetric to most asymmetric. Shown in this figure are systems with stellar masses $M_* > 10^{10} \, M_\odot$ at redshifts $2.2 < z < 3$. These galaxies are typically much smaller and bluer and have a higher asymmetry and inferred merger fraction than galaxies of comparable mass today (Conselice et al. 2008).

the triggering of AGNs and the formation of supermassive black holes. The observational studies above all locate bars within disks either through changes in ellipticity and position angle in the surface brightness profiles of galaxies or through visual inspection. It remains to be seen how the bar fraction holds when observed with a near-IR band such as within the CANDELS survey.

A related issue is finding the onset of spiral structure, which has remained a problem for a variety of reasons, but especially because of the difficulty of achieving an unambiguous detection owing to resolution/depth issues. Several papers published with the advent of ACS on HST showed that

there are many examples of disk-like morphological systems at high redshifts. This includes the disks found by Labbe et al. (2003), the Luminous Diffuse Objects of Conselice et al. (2004), and later systems identified by Elmegreen et al. (2007) as clump-clusters. More recently, Law et al. (2012a) discovered a galaxy with a likely bona fide spiral structure at $z = 2.18$ that also contained a large internal velocity dispersion based on integral field unit (IFU) spectroscopy. Spiral arms, however, appear very rare at high redshift, and likely only a small number are formed before $z \sim 1$. This is a major problem that needs more attention and could be addressed with recently available data. However, there are many galaxies with clumpy features that are potential spiral arms and disks in formation, which I discuss in detail in Section 4.4.

Another feature of spirals and disks is the formation of bulges. Although the traditional scenario is that bulges form in mergers (Section 4.3), recent results suggest that bulges can form in multiple ways. Pseudobulges are different from classical bulges in that they are likely formed through secular processes within a disk. This can be seen in the different correlations between bulge properties and central massive black holes (e.g., Graham 2008, Hu 2008, Graham & Scott 2013, Kormendy & Ho 2013).

Although morphology itself can often be ambiguous in terms of matching with contemporary Hubble types, IFU or long-slit spectroscopy can remove some degeneracies. In particular the use of integral field spectroscopy on $z > 1$ systems reveals important clues about the nature of these high-redshift galaxies (Förster Schreiber et al. 2009, Glazebrook 2013). Currently the most influential studies have been carried out with the SINFONI IFU on the VLT along with some work done with OSIRIS on Keck (Law et al. 2012a,b).

These surveys, most notably the SINS collaboration (e.g., Förster Schreiber et al. 2009) find an equal distribution of different kinematic classes that are rotationally dominated, mergers, and very compact galaxies with high velocity dispersions (e.g., Buitrago et al. 2014 for massive galaxies). The true nature of these systems is not yet known, although in general it appears that galaxies at $z > 2$, which are clumpy, tend to have high velocity dispersions. This perhaps reveals that the formation modes of disk galaxies at high redshift results in a high velocity dispersion. The future looks promising for combining larger surveys of IFU measurements of distant galaxies with resolved morphologies to decipher evolution. Large surveys with, for example, KMOS on VLT and MOSFIRE on Keck should revolutionize this area in the coming years.

4.2. Size and Profile-Shape Evolution

One of the most important findings in galaxy evolution studies in the past decade has been the discovery that distant galaxies are more compact than systems of the same mass in the local Universe (e.g., Daddi et al. 2005; Trujillo et al. 2007; Buitrago et al. 2008; van Dokkum et al. 2008, 2010; Weinzirl et al. 2011; Barro et al. 2013; Williams et al. 2014). Change in sizes with time is now well characterized, and the evolution of galaxy sizes at a constant stellar mass selection of $M_* > 10^{11} M_\odot$ can be characterized by a power law of the form $R_e \sim \alpha(1 + z)^\beta$. The value of the power-law slope changes with the galaxy surface brightness profile type such that the disk-like galaxies with Sérsic indices $n < 2.5$ evolve with $\beta = -0.82 \pm 0.03$, whereas spheroid-like galaxies with $n > 2.5$ have $\beta = -1.48 \pm 0.04$ (**Figure 11**). This demonstrates that there is a faster evolution in measured sizes for spheroid-like galaxies, which therefore have a more effective increase in size over cosmic time than the disk-like objects.

This size evolution is such that the effective radii of massive galaxies increases by up to a factor of five between $z = 3$ and today for galaxies at the same stellar mass (e.g., Buitrago et al. 2008, Cassata et al. 2013). The form of this evolution has been investigated to determine whether or

Lookback time (Gyr)
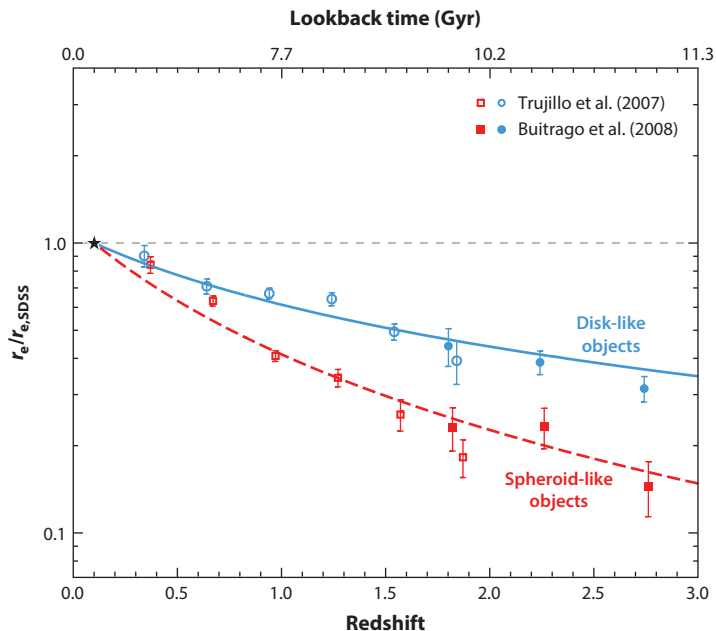
Figure 11

The average sizes of massive galaxies selected with $M_* > 10^{11} M_\odot$ as imaged in the POWIR (Conselice et al. 2007) $z < 2$ data and GOODS NICMOS survey (GNS) > 1.5 images (Buitrago et al. 2008, Conselice et al. 2011b). The size evolution is divided among galaxies with elliptical-like profiles, Sérsic indices $n > 2.5$, and disk-like profiles having $n < 2.5$. The measured effective radius, R_e, is plotted as a function of the ratio with the average size of galaxies at the same stellar mass measurements with $M_* > 10^{11} M_\odot$ at $z = 0$ from Shen et al. (2003).

not the increase is due to the buildup of the entire galaxy or just the inner or outer parts. The data to date show that galaxy growth through sizes is occurring in its outer parts, with the central parts in place at early times (e.g., Carrasco et al. 2010, van Dokkum et al. 2010). This indicates that the buildup of massive galaxies is an inside-out process, whereby the inner parts of massive galaxies are in place before the outer parts in galaxies with the same stellar mass density as today (e.g., Hopkins et al. 2009).

An alternative way to investigate this problem is to examine the number of compact and ultracompact galaxies at various redshifts. There is some controversy over whether or not there exist in the local Universe compact galaxies with sizes similar to those seen at high redshifts. However, what is clear is that the number densities of these ultracompact galaxies declines in relative abundance very steeply at $z < 2$ (Cassata et al. 2013).

The processes responsible for this increase in sizes at lower redshifts is not well understood and is currently a source of much debate. The most popular explanation is that this size increase is produced through minor mergers (e.g., Bluck et al. 2012, McLure et al. 2013), although other ideas such as AGNs performing work on gas is another idea (e.g., Bluck et al. 2011). However, the outer parts of nearby massive galaxies are too old to have been formed in relatively recent star formation, and the star formation observed at high redshift is not sufficient to produce the observed increase in sizes (Ownsworth et al. 2012).

The major idea for the physical mechanism producing galaxy-size evolution is through dry minor mergers, as major mergers are not able to produce the observations of increasing size

without significantly increasing mass (e.g., Khochfar & Silk 2006, Naab et al. 2009, Bluck et al. 2012, Oser et al. 2012, Shankar et al. 2013). There is currently some controversy over whether or not the observed minor merger rate is high enough to provide this increase in sizes, with the most massive galaxies of $M_* > 10^{11}\,M_\odot$ appearing to have enough minor mergers (e.g., Kaviraj et al. 2009) to produce this size evolution (Bluck et al. 2012), but this may not be the case for lower-mass systems (e.g., Newman et al. 2012). It does appear, however, that minor mergers are a significant mechanism for producing low levels of star formation in early types at $z \sim 0.8$ as well as for adding significant amounts of stellar mass to these galaxies (Kaviraj et al. 2009, 2011). Alternatively, the compact high-z galaxies may evolve into bulges of modern large spiral galaxies (e.g., Graham 2013, Dullo & Graham 2013). One of the major issues is determining not only the number of minor dry mergers but also the timescale for these mergers (Section 3.4), which more simulations would help elucidate.

Along with the evolution of galaxy sizes, there is also significant evolution in the underlying structures of galaxies at higher redshifts. One of the cleanest ways to see this is through the evolution of the Sérsic parameter, n (**Figure 7**). When examining the evolution of derived values of n as a function of redshift both for a stellar mass and at a constant number density selection, it is apparent that galaxies have lower n values at higher redshifts for the same selection (e.g., Buitrago et al. 2013). This has been interpreted by some to imply that these galaxies are more "disk-like" at high redshifts (Bruce et al. 2012), although the morphologies of these systems by visual inspection, and their internal structures and colors, are not similar to modern disks (e.g., Conselice et al. 2011a, Mortlock et al. 2013). These disk-like galaxies, while having light profiles similar to modern disks, are much smaller, have a higher stellar mass, and are often undergoing intense star formation with peculiar morphologies, making them undisk-like in all other regards. They are indeed likely a type of galaxy with no local counterpart.

4.3. The Merger History

One of the primary, if not the primary, uses of galaxy structure at high redshift at the time of writing is to measure the merger history of galaxies. This is a major issue in extragalactic astronomy, as merging is not only a method for galaxies to form but is also a potential way in which black holes, star formation, and other internal features of galaxies are assembled. Merging is also one of the key predictions of the cold dark matter model, which is the dominant idea for how galaxy evolution occurs through cosmic time (e.g., White & Rees 1978, Blumenthal et al. 1984, Cole et al. 2000).

The merger history of galaxies was first measured using galaxies in pairs—systems of at least two galaxies near enough to each other to merge in a reasonable amount of time (typically 20 or 30 kpc) and in cases of kinematic pairs with a low velocity difference of around 200 km s^{-1} (e.g., Patton et al. 1997, 2002; Le Fèvre et al. 2000; Lopez-Sanjuan et al. 2011, 2012). Simulation results show that most pairs of galaxies selected in this way will eventually merge within a timescale comparable to dynamical friction (e.g., Moreno et al. 2013). Using pairs to find galaxies that are merging is still a large industry, and interested readers are referred to the latest papers in this field (e.g., Lopez-Sanjuan et al. 2011, 2012; Tasca et al. 2014). Pairs of galaxies also provide a check on the methodology we use to find major mergers, as it is an independent measure of this formation mode. However, the merger fraction measured through pairs is more statistical in nature than structure and does not reveal for certain whether a galaxy is a merger or not.

A detailed CAS structural study of starburst, ULIRGs, and other merging galaxies shows that another route for measuring the merger history is through the use of the asymmetry index, whereby the most asymmetric galaxies are ones involved in mergers (Conselice 1997, 2003; Conselice et al. 2000a,b; Bridge et al. 2007) (Section 3.2). The merger history is also measured through other
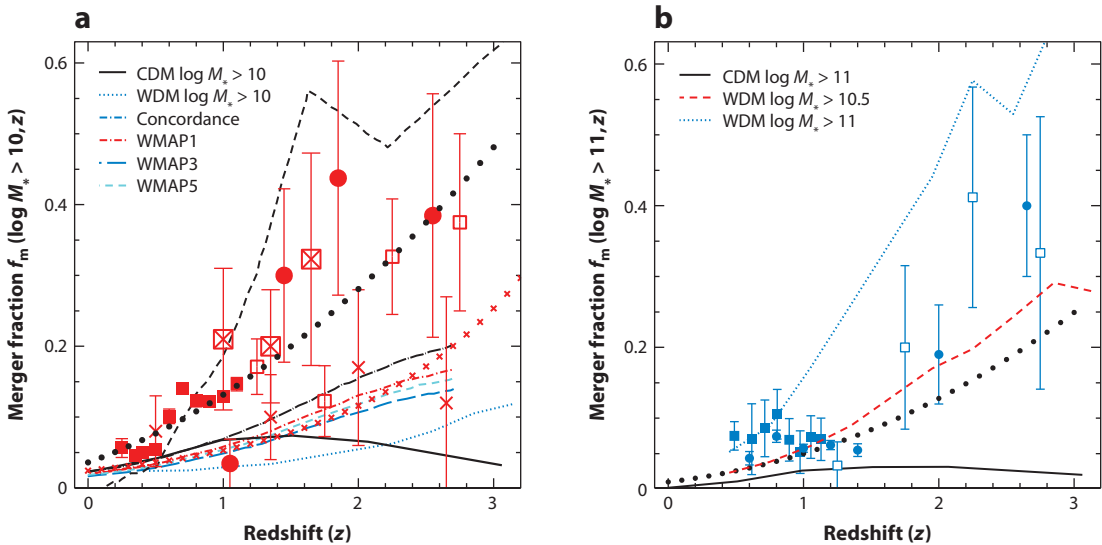
Figure 12

A compilation of the merger fraction history for galaxies selected with stellar masses $M_* > 10^{10}\,\mathrm{M}_\odot$ and $M_* > 10^{11}\,\mathrm{M}_\odot$. (*a*) Points shown here are for $M_* > 10^{10}\,\mathrm{M}_\odot$ galaxies, including results from Conselice et al. (2003a) at $z > 1$ in the Hubble Deep Field (*solid circles*); from Conselice (2009) at $z < 1.2$ (*solid boxes*); and from Mortlock et al. (2013) at $z > 1$ (*open boxes*). Also shown are pair merger fractions at separations of <30 kpc: from Man et al. (2012) at $z > 1$ (*crosses*) and from Lopez-Sanjuan et al. (2010) (*large open boxes with crosses*). (*b*) The merger history for $M_* > 10^{11}\,\mathrm{M}_\odot$ systems, including results from Conselice (2009) at $z < 1.2$ (*solid boxes*); from Bluck et al. (2009, 2012) at $z > 0.5$ (*solid circles*); and from Mortlock et al. (2013) at $z > 1$ (*open boxes*). In both panels, the line with the dark solid circles is the best fit relation for a merger fraction parameterization as $\sim (1+z)^m$. The blue dotted lines in both panels *a* and *b* and the red dashed line in panel *b* show the predicted merger history within warm dark matter (WDM) simulation predictions at the labeled respective masses. The solid black line shows the corresponding predictions from cold dark matter (CDM) simulations. For the $M_* > 10^{10}\,\mathrm{M}_\odot$ panel I also show the merger fraction calculation from abundance matching using various WMAP and concordance cosmologies as well as abundance matching from Stewart et al. (2008) (line made up of *red crosses*).

parameters, whereby mergers occupy a unique parameter space (e.g., Lotz et al. 2004, 2008a; Freeman et al. 2013).

Although there is no perfect 1:1 relation between parameter space definitions of mergers with all mergers identifiable by eye, we still find that about half of all identifiable mergers fall within specific regions of parameter space and that there is low contamination from other galaxy types (Section 3.2). Thus, galaxy merger fractions are observations that have to be interpreted carefully with the use of galaxy merger models.

4.3.1. The merger fraction evolution. The merger fraction history is the basic observable that reveals how mergers are changing and evolving through cosmic time. It is measured at high redshift through the criteria described in Section 3.2, and the resulting merger fractions are shown in **Figure 12** (e.g., Conselice et al. 2008, 2009; Bluck et al. 2012). This figure shows that the inferred merger fraction increases with redshift. This increase is typically fit as a power law of the form

$$f_{\mathrm{m}} = f_0 \times (1+z)^m, \tag{14}$$

where f_0 is the merger fraction at $z = 0$ and m is the power-law index for measuring mergers. In general, the higher the value of m the more steeply the merger history increases at higher redshifts. An alternative parameterization of the merger history is given by a combined power-law

exponential (e.g., Conselice et al. 2008), whose form is

$$f_{\mathrm{m}} = \alpha \times (1 + z)^m \exp[\beta(1 + z)]. \tag{15}$$

The local $z = 0$ merger fraction in this formalism is given by $f_{\mathrm{m}}(0) = \alpha \exp(\beta)$, and the merger peak is located at $z_{\mathrm{peak}} = -(1 + m/\beta)$. This form of the merger fraction evolution appears to fit lower-mass galaxy merger fractions better than a single power law up to $z \sim 3$, as this allows for a merger fraction peak and a decline at higher redshifts. In fact, only the highest-mass galaxies with $M_* > 10^{10}\,M_\odot$ appear to increase up to $z \sim 3$, whereas lower-mass galaxies have a merger peak around $z \sim 1.5$–2.5, which declines at higher redshifts (e.g., Conselice et al. 2008).

Although initially there were significant differences in merger histories between different studies (e.g., Lin et al. 2004), it is now clear that these are due to several effects. The first is that the value of the power-law index m can vary significantly just due to the value of the anchor redshift at $z = 0$. Secondly, when comparisons are done between galaxies that have been selected in the same way (stellar mass or absolute magnitude), and correct timescales are used for different techniques (Section 3.4), then merger rates agree within the uncertainties (e.g., Conselice 2009, Jogee et al. 2009, Lotz et al. 2011).

The merger history tends to peak at $z \sim 2.5$ for massive galaxies with $M_* > 10^{10}\,M_\odot$ at values of $f_{\mathrm{m}} \sim 0.3$–0.4 and decline at lower redshifts. The values for m found in the literature can vary significantly, but most of this is due to different selections and different redshift ranges used as well as the use of various values for the local merger fraction. The first studies using pairs found a very steep increase up to $z \sim 1$, with $m = 2.8 \pm 0.9$ for a luminosity-selected sample up to $z \sim 0.4$ (Patton et al. 1997). The value of m was later found by Patton et al. (2002) to be $m = 2.3 \pm 0.7$ within the CNOC2 redshift survey up to $z \sim 0.55$. Le Fèvre et al. (2000) measure the merger fraction using 285 galaxies in the Canada-France Redshift Survey and the Low Dispersion Survey Spectrograph surveys up to $z \sim 1$, finding a power-law index of $m = 3.2 \pm 0.6$, although this lowers to $m = 2.7 \pm 0.6$ after considering selection effects. Other studies have found similar values, with $m = 1.5 \pm 0.7$ for brighter galaxies in the VIMOS VLT Deep Survey (de Ravel et al. 2009), and $m = 3.1 \pm 0.1$ for pairs up to $z \sim 1$ in the COSMOS field (Kartaltepe et al. 2007). These are, however, all relatively nearby galaxies at $z < 1$. For higher redshifts, Bluck et al. (2009) find a power law of $m = 3.0 \pm 0.4$ for galaxies with $M_* > 10^{11}\,M_\odot$ using pairs from the GOODS NICMOS survey.

Within morphological studies, Conselice (2003) finds a high m index of $z \sim 4$ for massive galaxies with $M_* > 10^{10}\,M_\odot$, with m values around $m \sim 1$–2 for lower-mass galaxies. This is similar to what is found by Le Fèvre et al. (2000) when examining the merger history of visually disturbed galaxies in Hubble imaging. This was confirmed by Conselice et al. (2008) using the same methods, but on the Hubble UDF data. Conselice (2003) also shows how the merger fraction slope m can vary significantly depending on what redshift limit is used and whether stellar mass or luminosity cuts are applied to the selected sample. In a detailed study of $z < 1$ galaxies from the COSMOS survey, Conselice (2009) finds an index of $m = 2.3 \pm 0.4$ for galaxies with stellar masses of $M_* > 10^{10}\,M_\odot$. By contrast, Lotz et al. (2008a) find that the merger fraction does not evolve significantly with redshift in the range of $z \sim 0.2$–1.2, with a weak increase in the merger fraction with $m = 0.23 \pm 1.03$ using the Gini/M_{20} methods. Later, however, it was shown that Gini/M_{20} is very sensitive to minor mergers, and once these effects are considered the fitted parameter is $m = 2$ up to $z \sim 1.2$ (Lotz et al. 2011). Other methods of measuring the merger or interaction rate include looking for ringed galaxies (D'Onghia et al. 2008), a method that derives a merger fraction index with $m \sim 3$.

4.3.2. Galaxy merger rate evolution.

The merger fraction is simply just an observational quantity, as it is the fraction of galaxies in a sample that have merged with another galaxy. This merger fraction can effectively be anything from zero to near unity depending on the mass ratio and timescales of interest. Merger fractions must therefore be carefully interpreted. The physical quantity we are interested in is the merger rate, which gives the number of mergers occurring per unit time and in some cases per unit volume per unit time.

Bluck et al. (2012), Lotz et al. (2008a), Jogee et al. (2009), and Conselice (2006b) show that CAS is only sensitive to major mergers of mass ratios of 4:1 and lower and has a particular timescale of about ~0.5 Gyr associated with the merger sensitivity (Section 3.4). This is very similar to the merger parameter sensitivity when using pairs of galaxies with mass ratios of 4:1 or lower (i.e., major pairs). Thus, by examining the merger fraction with CAS, we are likely tracing the same systems as measured through galaxies in pairs.

The merger fraction is converted into a galaxy merger rate through the use of the merger timescale τ_m, which can be derived through simulations (Lotz et al. 2010a) (see Section 3.4) or through the decline in the merger fraction at lower redshifts (Conselice 2009). The result of both approaches is that the CAS merger timescale is around 0.5 Gyr for a galaxy to remain "peculiar" in parameter space; the merger timescale in Gini/M_{20} remains at a similar level, but is more sensitive to minor mergers (Section 3.4).

Using the merger timescale, the merger rate per galaxy is thereby defined by the parameter Γ (e.g., Bluck et al. 2009, Conselice 2009),

$$\Gamma(M_*, z) = \frac{\tau_m}{f_{gm}}. \tag{16}$$

The value of Γ is in units of gigayears and gives the average amount of time between mergers for a galaxy within the given selection property, typically stellar mass, and within a given redshift range. Note that within the definition of Γ the galaxy merger fraction is used rather than the merger fraction (Section 3.2). The value of Γ as a function of redshifts for CAS merger measures and the pair selection mergers sample is shown in **Figure 13**.

Using the evolution of the galaxy merger rate, per galaxy, Γ, the number of mergers that occur between various redshifts is calculated by integrating the inverse of Γ over redshift,

$$N_{merg} = \int_{t_1}^{t_2} \Gamma^{-1} dt = \int_{z_1}^{z_2} \Gamma^{-1} \frac{t_H}{(1+z)} \frac{dz}{E(z)}. \tag{17}$$

The result of this is studied in detail by Conselice (2009) and Bluck et al. (2009); initial results using simulations are discussed by Conselice (2006b). The result of these calculations shows that the number of major mergers a galaxy undergoes between $z = 3$ and $z = 1$ is 4.3 ± 0.8 major mergers at $z < 3$ (Conselice et al. 2008) for galaxies selected with stellar masses $M_* > 10^{10} M_\odot$. There also appears to be a limited number of mergers at higher redshifts of $z > 3$ (Conselice & Arnold 2009).

The Γ definition of the merger rate is per galaxy and thus does not take into account the overall merger rate within the Universe. Thus ultimately we are interested in the galaxy merger rate, $\Re(M_*, z)$:

$$\Re(M_*, z) = f_{gm} \tau_m^{-1} n_m, \tag{18}$$

where n_m is the number density of galaxies at a given redshift. Although this is the ultimate quantity in galaxy merger studies, it is difficult to measure, and the number density, n_m, has its own associated uncertainties (e.g., Mortlock et al. 2011). In **Figure 13**, we plot the merger rate for galaxies using the CAS systems for pairs and mergers using the number densities of galaxies from Mortlock et al. (2011).
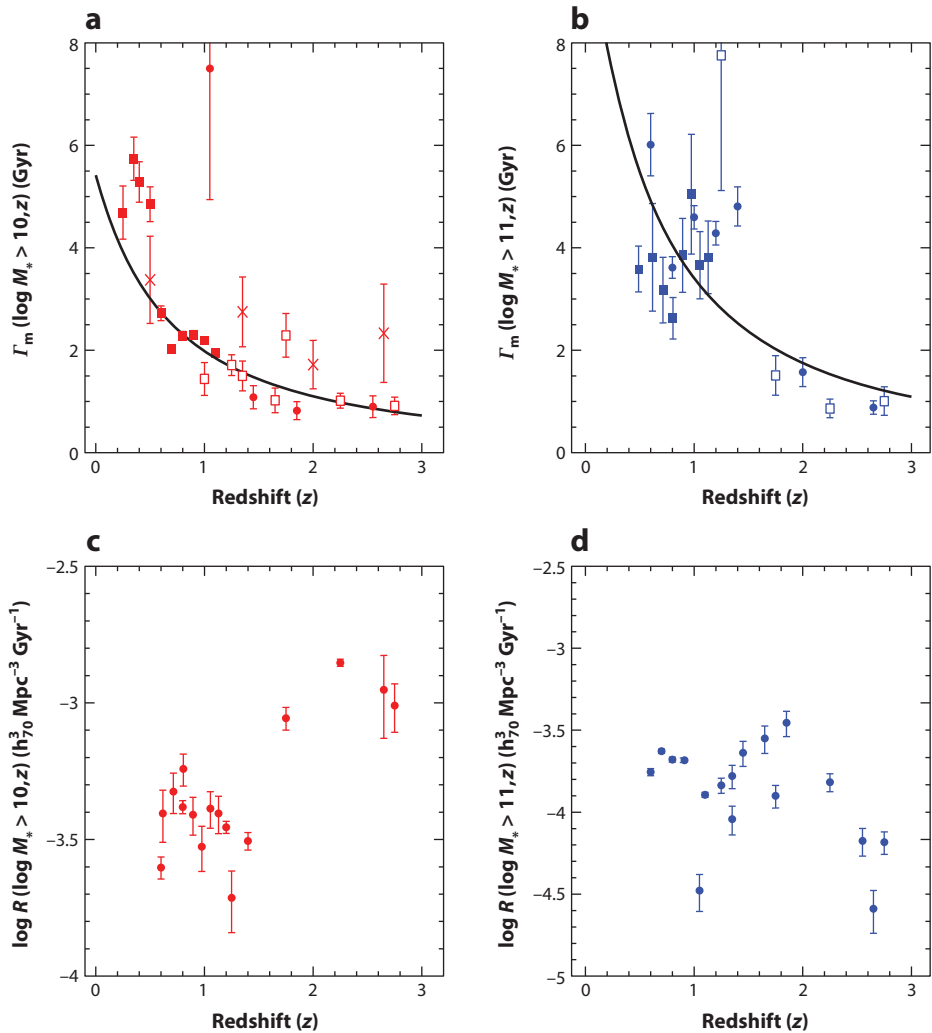
Figure 13

The merger rate for galaxies plotted in two different ways. The upper panels plot the merger rate per galaxy, (*a*) $\Gamma(z)$ at stellar mass limits of $M_* > 10^{10}\,M_\odot$ and (*b*) $M_* > 10^{11}\,M_\odot$. The units of Γ are in gigayears and represent the average time between mergers for a typical galaxy at the given mass limit. (*c,d*) The ultimate realization of the merger rate is shown at these two stellar mass limits, as the number of mergers occurring per gigayear per comoving cubic megaparsec. The point types in the merger rate per galaxy have the same meanings as the merger fraction plot in **Figure 12**.

Although the number of mergers is an interesting and fundamental quantity, we are ultimately interested in the amount of stellar mass added from mergers to galaxies over time. The total amount of stellar mass accreted into a galaxy is calculated as a double integral over the redshift range of interest (z_1 to z_2 or lookback times t_1 and t_2) and over the stellar masses range that is being probed (M_1 to M_2), and can be expressed as

$$M_{*,M} = \int_{t_1}^{t_2} \int_{M_1}^{M_2} M_* \times \frac{f_m'(z, M_*)}{\tau_m(M_*)} dM_* dz, \qquad (19)$$

where $\tau_m\,(M_*)$ is the merger timescale, which depends on the stellar mass of the merging pair (Bluck et al. 2012). From this we calculate the total integration of the amount of mass assembled through merging for galaxies with stellar masses $M_* > 10^{11}\,M_\odot$. For a $z < 3$ mass complete sample at this limit, Conselice et al. (2013) find a value $M_{*,M}/M_*(0) = 0.56 \pm 0.15$, where $M_*(0)$ is the initial average stellar mass at $z \sim 3$, and $M_{*,M}$ is the average amount of stellar mass accreted in mergers at $z = 1$–3. This ratio is the fractional amount of stellar mass added due to both major and minor mergers for systems with stellar mass ratios down to 1:100 for an average massive galaxy after a merger adjusted for constant comoving density (Conselice et al. 2013). By observing the number of mergers, we can get an idea of how much gas is added to galaxies through the merger process. Comparing this with the star-formation rate, there is a large deficiency, which must be accounted for by gas accreted from the intergalactic medium. Using this number and the observed star-formation rate within these galaxies, the gas accretion rate from the intergalactic medium is calculated at around $100\,M_\odot\ year^{-1}$, adding roughly the same amount of stellar mass to these galaxies as mergers (Conselice et al. 2013).

## 4.4. Resolved Morphological Formation Histories

Independent of the formation of the gross, or bulk, galaxy structure is the formation of their stars and how this correlates with structure and its assembly. This is effectively done by examining the SEDs of individual components in galaxies (i.e., disks or bulges) and/or using a newer technique of examining the SEDs of individual pixels. With resolved imaging it is therefore possible to determine to some extent the star-formation history of individual resolution elements (e.g., Abraham et al. 1999a, Zibetti et al. 2009) as well as the stellar mass within these (e.g., Lanyon-Foster et al. 2007).

Using early results from small samples of a few dozen galaxies at $z \sim 1$, Abraham et al. (1999a) demonstrated that many morphologically selected ellipticals in their sample show a diversity in their star-formation histories, with recent bursts of star formation commonly seen. Abraham et al. (1999a) also showed that bulges in these systems almost always have ages older than their disks. This was followed up with a study of 79 field spheroids by Menanteau et al. (2001), who found that a third of their morphologically regular systems have recent star formation in their centers, with so-called blue cores. It is possible that some of these systems are forming the pseudobulges that we see in the nearby Universe.

There are other studies of the bulges of distant galaxies, including that by Hathi et al. (2009) who find that bulges at $0.8 < z < 1.3$ have ages of 1–2 Gyr, with stellar masses up to $10^{10}\,M_\odot$ in the Hubble UDF. They also find that late-type bulges are younger than early types, a finding that also exists in the local Universe. However, classical bulges up to $z \sim 1$ with de Vaucouleurs profiles are found to have old stellar populations similar to giant ellipticals at the same epoch (Koo et al. 2005).

Another potentially powerful approach toward understanding the formation history of galaxies is to examine their light distribution on a pixel-by-pixel basis. The idea here is that each pixel or resolution element is independent of others and each has their own SED that can be fit by stellar population analysis methods (e.g., Bothun 1986, Abraham et al. 1999a, Lanyon-Foster et al. 2007). Local galaxies have different pixel color magnitude diagrams, depending on morphological type, with early types having a much more narrow locus of points than disk galaxies.

Galaxies also often look more symmetrical in stellar mass maps than in light (Lanyon-Foster et al. 2012, Wuyts et al. 2012; **Figure 14**). Star-forming galaxies in the CANDELS survey were recently studied in a pixel-by-pixel approach by Wuyts et al. (2012), who examined 323 systems at $0.5 < z < 1.5$ and a further 326 higher redshift systems at $1.5 < z < 2.5$. This study uses the optical ACS and near-IR WFC3 filters to construct SEDs for all pixels in these galaxies. Wuyts
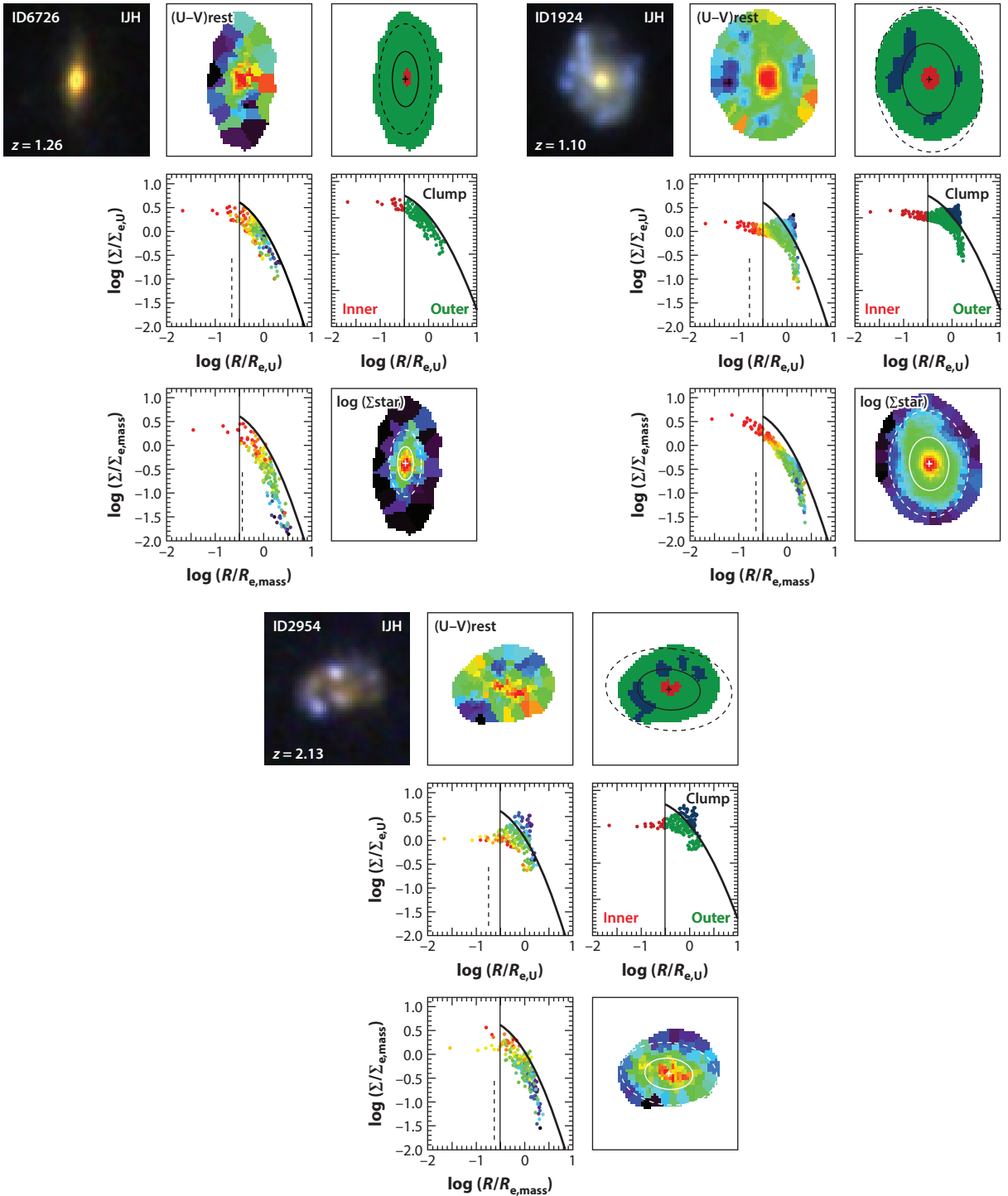
et al. (2012) find that the nuclei of star-forming galaxies are redder and have older ages than their outer parts. Clumps in these galaxies also generally occupy a smaller fraction of the total mass than the total light, demonstrating that the large clumps seen in distant star-forming galaxies are mostly star-forming regions. Clumps are also found to be central, off-central, or outer, and these clumps may play a role in forming the bulges of these galaxies through a secular process (Bournaud et al. 2007, Elmegreen et al. 2008, Genzel et al. 2008) (Section 5). This shows that there are methods beyond hierarchical clustering for the formation of structures within galaxies.

4.5. High-Redshift Active Galactic Nuclei/Starbursts and Star-Formation Quenching

One of the major ideas behind how mergers drive galaxy formation is that when galaxies merge, gas clouds collide, triggering star formation. At the same time, gas is driven to the centers of galaxies, producing AGN (e.g., Hopkins et al. 2008). Observationally we also know that galaxies that are concentrated, with for example a high Sérsic profile, are more likely to be quenched (e.g., Bell et al. 2012, Fang et al. 2013). There is therefore a strong theoretical reason to expect that structure, as influenced by mergers, should correlate with galaxy formation. There is also strong evidence that the star formation in galaxies is regulated by structure. How these relate, however, is not yet clear.

Observationally it has proven thus far difficult to correlate the presence of mergers, through either pairs or the presence of distorted or peculiar structures, with the presence of AGN or a star-formation excess at high redshift. Recent studies such as that by Cotini et al. (2013) use CAS indices to show that the fraction of nearby galaxies with AGN are roughly five times more likely than a control sample to have a distorted structure. However, studies at higher redshifts generally do not find that more asymmetric or merging galaxies have a higher AGN fraction (e.g., Grogin et al. 2005, Gabor et al. 2009, Kocevski 2012). This is also found in the deepest ACS Hubble imaging, although it does appear that AGN are found in more concentrated galaxies at higher redshifts (Grogin et al. 2005). There is also a lack of a higher fraction of peculiar/merging galaxies found in the GEMS/STAGES HST survey by Bohm et al. (2013) for AGN with luminosities of $L_X < 10^{44}$ erg s^{-1}. This may be an indication that Type 1 AGN are more likely found in early-type massive systems. It remains to be seen if obscured AGN, the Type 2s, are found in more merging systems and thereby represent an earlier phase of the merger.

Another major issue in which morphology and structure play an important role is understanding the origin of dusty star-forming galaxies, the so-called ULIRGs or submillimeter galaxies. Submillimeter galaxies are those that appear very bright at submillimeter wavelengths, typically

---

Figure 14

Internal pixel structures and profiles for galaxies at $z \sim 1$–2 with and without star formation. The examples are ID6726, which is a nonstar-forming galaxy, and ID1924 and ID2954, which contain clumpy star-forming knots throughout their structures. These are representative examples of commonly found galaxies at high redshifts, typically around $z \sim 2$ as seen in deep WFC3 images from surveys such as CANDELS. For each of these galaxies, the top rows demonstrate the image in the IJH *Hubble Space Telescope* bands, the rest-frame (UV) color map, and a map that indicates whether pixels belong to the inner (*red*), outer (*green*), or clump region (*dark blue*) for each galaxy. The solid black ellipses show the area that contains half of the rest-frame *U*-band light for each system. The middle rows for each galaxy show the *U*-band light profile, which is color coded on the left by the pixel type labeled in the (*U*−*B*) color map and on the right by the location of the various pixels. The lines shown in the middle row panels show the separation between the different spatial distributions. The bottom rows show the distribution in terms of stellar mass. The vertical dashed lines show the resolution limit of WFC3. The final panels show the stellar mass map for each system, with the inner solid and outer dashed lines showing the location of $R_{e,mass}$ and $2R_{e,mass}$. Reprinted from Wuyts et al. (2012) with permission and courtesy of Stijn Wuyts.

at 850 μm, and are at high redshift at $z > 1$. Morphological analyses of these submillimeter galaxies showed early on that they are involved in merger activity and have peculiar morphologies (e.g., Chapman et al. 2003, Conselice et al. 2003b). Many of these galaxies have structures and morphologies consistent with being involved in mergers (e.g., Ricciardelli et al. 2010). Kartaltepe et al. (2012) find that a sample of ULIRGs selected from the CANDELS fields are more likely than a field galaxy sample to be involved in galaxy interactions and mergers (72^{+5}_{-7}% versus 32 ± 3%). However, Swinbank et al. (2010) argue, using a large sample of submillimeter galaxies, that their morphologies are not significantly different from other star-forming field galaxies at similar redshifts. Swinbank et al. (2010) also find that their submillimeter galaxies have light profiles more similar to early types rather than disks. Although, Targett et al. (2011) find that submillimeter galaxies have disk-like profiles and conclude that these systems are more like forming disks than forming spheroids in mergers. This suggests that the morphology of submillimeter galaxies is still open for debate, and results appear to be conflicting. More detailed work, likely with adaptive optics in the K-band to avoid issues with dust and morphological k-corrections, are needed to make further progress.

Furthermore, as mentioned earlier, there is a strong observed correlation between galaxies that have steep surface brightness profiles, with $n > 2.5$, and the quenching of star formation (e.g., Bell et al. 2012). This shows that galaxy structure either produces a change in the galaxy history or more likely is a symptom of the effects that produce this quenching. In general, there are a few ways to quench the star formation seen in galaxies at high redshift. Some of these are environmental, such as ram-pressure stripping and strangulation (e.g., Peng et al. 2010). However, these processes are ineffective for the bulk of the field galaxies that we study in this review. What is more likely is that quenching of typical field galaxies is merger driven or it is driven by the stellar/halo mass in some form of feedback process (e.g., Peng et al. 2010, 2012; Carollo et al. 2013; Lilly et al. 2013). The most likely candidates are mergers that either heat gas or remove most of it in giant starbursts, preventing further star formation. The other idea explaining this feedback is that it is the result of AGNs, whereby the ongoing star formation is truncated by the existing gas in a galaxy being heated or removed by an active AGN (e.g., Croton et al. 2006). It is therefore likely that a few critical processes are ongoing to produce the Hubble sequence, specifically the red, passive and concentrated high-mass systems.

4.6. The $z \sim 3$–6 Frontier

By far the bulk of what we know of galaxy structural evolution is at $z < 3$. The reason for this is simply because this is the limit where we can observe the rest-frame optical using observations in the near-IR from the HST, which is only effective at imaging with filters bluer than the H-band (often H_{160} with WFC3 and NICMOS). However, there are some observations of galaxy structure at even higher redshifts that provide some information about the formation of these galaxies. To date most of these observations are done with a red filter using the ACS camera on HST, either the I_{814} or z_{850} band. It must be remembered that these systems are being observed in the rest-frame UV, and thus their morphologies are dominated by young stars.

There have only been a few major studies that focus on the structures of these ultrahigh-redshift galaxies. Ferguson et al. (2004) study the sizes and the axis ratios of Lyman-break galaxies (LBGs) galaxies up to $z \sim 6$ in the GOODS fields, finding that galaxies are smaller and more "disk-like" in their axis ratios at higher redshifts. This was also shown in an extensive study of 4,700 LBGs by Ravindranath et al. (2006), who find that 40% have exponential light profiles, 30% have de Vaucouleurs profiles, and the remaining 30% have multiple cores. The ellipticity distribution of these LBGs shows that these systems are skewed toward high values with $\epsilon > 0.5$, which cannot

be explained by viewing disks and spheroids at various angles (Ravindranath et al. 2006). This is either an indication that these systems are mergers or that star formation is distributed in the outer parts of these galaxies, thus creating these high-ellipticity structures.

For ultrahigh-redshift galaxies, Conselice & Arnold (2009) examine the visual morphologies and pair fractions of LBGs in the Hubble UDF ACS filters from $z \sim 4$–6. These ACS data on the UDF still provide the highest resolution and deepest imaging of the most distant galaxies. Conselice & Arnold (2009) find that the fraction of $z \sim 3$–6 LBGs that are peculiar in appearance is roughly constant at ~30% throughout this redshift range. Conselice & Arnold furthermore demonstrate that many of the LBGs at these redshifts have tidal-like features—fans, shells, etc.— that resemble merger signatures seen at lower redshifts. The derived merger fraction from LBG pairs also agrees with the merger fraction based on CAS and visual estimates (Conselice & Arnold 2009, Cooke et al. 2010).

It is perhaps surprisingly easier to identify galaxies in pairs at these redshifts than at lower redshifts, as one can use the drop-out band to remove contamination, and thus ensure that two galaxies close by in the sky are at least at a similar redshift. This results in a smaller correction being needed to calculate merger fractions, and thus the merger fraction in principle can be measured more accurately (Conselice & Arnold 2009). Jiang et al. (2013) similarly examine the rest-frame UV morphologies of 51 Lyman-α galaxies and 16 LBGs and find a merger fraction for the brightest galaxies of around 50% and otherwise a diversity in morphology.

Most recently, using WFC3 data from the UDF, Oesch et al. (2010) show that $z \sim 7$–8 galaxies are very compact; these systems have a typical size of 0.7 $\pm$ 0.3 kpc with little size evolution down to $z \sim 6$. There is more development down to $z \sim 4$, with the observation of more extensive wings of light at these lower redshifts, and a corresponding increase in sizes (e.g., Ferguson et al. 2004) following a similar power law with redshift, as is found for size evolution between $z \sim 3$ and $z \sim 0$ (Buitrago et al. 2008, Mosleh et al. 2012).

4.7. Role of Environment in Structure Formation

Galaxy morphology is well known to correlate strongly with environment in the local Universe (e.g., Dressler 1984, Postman et al. 2005). It is also clear that there is a strong relationship between morphology and stellar mass such that the most massive galaxies tend to have elliptical morphologies and lack star formation. Combining this with the morphology-redshift relation shows that the structure of a galaxy depends upon its mass and local environment as well as time. Which of these is the leading cause for producing galaxy evolution is an active area of study.

The problem of galaxy morphology as a function of density is a large area of research and is outside the immediate scope of this review. However, it is relevant to discuss some of the major findings and how they relate to the evolution of galaxy structure with time. The major effect of morphology is that the type of galaxy, either elliptical or spiral, depends to a large degree in the nearby Universe on the local density of that particular galaxy's environment. This relation is such that the higher the density of the local environment, the more likely a galaxy is early type and nonstar-forming (e.g., Dressler 1984, Gomez et al. 2003, Blanton & Moustakas 2009). Disk properties are also highly environmentally driven, with few classical bulge or elliptical systems in low-density environments (Kormendy et al. 2010).

It is also the case that more massive galaxies are more likely to be early type. The question is which relationship is more fundamental, and this relates to the old issue of "nature versus nurture" for galaxy formation. The structures and morphologies of galaxies can help address this problem, especially by examining the limited number of observations we have of galaxy structure in high-redshift overdensities or (proto)clusters.

Observations of overdensities at high redshifts are just starting in earnest, but already provide some clues. Very massive clusters at high redshifts, up to $z \sim 1.2$, contain a similar pattern of morphologies and densities as local galaxies, such that the denser areas contain a higher fraction of systems that are elliptical. This tends to break down for the limited number of cluster candidates found at higher redshifts, where the galaxy population is irregular and peculiar, as is found for the general high-redshift galaxy population (e.g., Papovich et al. 2012).

Detailed studies are, however, possible up to $z \sim 1$ by both using field galaxies of various local environments as well as looking at the morphological and structural distributions of galaxies within rich clusters at various redshifts. For field galaxies, Tasca et al. (2009) examine the morphology-density relationship for 100,000 galaxies in the COSMOS survey. They find that the morphology-density relation changes slightly with redshift, becoming flatter at higher z (e.g., Grützbauch et al. 2011a,b). Above a stellar mass of about $10^{10.6} \, M_{\odot}$ the morphologies of galaxies appear to become more dominated by the stellar mass as the critical factor rather than density (e.g., Grützbauch et al. 2011b). The situation in rich clusters at $z \sim 1$, and the formation of S0s, is such that the trend with environment is not as steep as is found at $z \sim 0$. This suggests that S0s are not entirely formed yet in these distant clusters; however, the elliptical population does seem to be in place compared with the population at $z \sim 0$.

Another structural feature that can be investigated is the size evolution and how it varies with environment. The limited number of investigations of this have found that galaxies at $z > 1$ in higher-density environments show signs of a more rapid increase of galaxy size with redshift in comparison with the field (e.g., Cooper et al. 2012, Lani et al. 2013). This is one indication whereby a dense environment can facilitate a more rapid evolution in galaxies, although it is a slight effect that needs further confirmation.

5. COMPARISONS TO THEORY

Examination of galaxy morphology and structure provides a new perspective to compare against cosmologically based galaxy formation models, including those that entail extensive physics, such as star formation, AGN feedback, and supernovae, in more detailed hydrodynamical models. This review only briefly discusses this large topic and how it relates to galaxy structure. For a more detailed recent review on the theory of galaxy formation from a theoretical prospective, see Silk & Mamon (2012).

Galaxy formation models were first developed to explain the structures of galaxies, namely the bulge/disk/halo trichotomy, and the ages of the stars in these components (Eggen et al. 1962). The default initial assumption in the first galaxy formation models was that galaxies formed like stars in a relatively rapid collapse. In the 1980s the first computer simulations of structure formation showed that a Universe dominated by cold dark matter (CDM) matched observations of galaxy clustering on large scales (Davis et al. 1985) and that within this framework galaxy assembly should be hierarchical (Blumenthal et al. 1984), yet this is a fundamental prediction that is just now starting to be tested with only a few papers comparing the observations with the theoretical predictions (e.g., Bertone & Conselice 2009, Jogee et al. 2009, Hopkins et al. 2010, Lotz et al. 2011).

Today there are many simulations used to predict properties of the galaxy population and how it evolves through time. These models are largely successful when predicting basic properties of nearby galaxies, such as their luminosities, masses, colors, and star-formation rates, as well as the evolution of galaxy scaling relationships. However, problems still exist in predicting the abundances of low- and high-mass galaxies (e.g., Conselice et al. 2007, Guo et al. 2011). Within galaxy-formation models there are very famous problems such as the satellite and the CDM dark matter profile, but there are also significant issues when examining how the evolution of galaxies

occurs and trying to match this with the theory. Another major problem is that there are several large disk galaxies without significant bulges in the nearby Universe that are not predicted in CDM (e.g., Kormendy et al. 2010).

One of the ways to further test these models is to investigate how well CDM models can reproduce the formation history of galaxies as seen through the merging process using the so-called semianalytical method (e.g., Bower et al. 2006, Guo et al. 2011). We show this comparison with the measured merger fractions in **Figure 12** at two different stellar mass ranges of $M_* > 10^{10}\,M_\odot$ and $M_* > 10^{11}\,M_\odot$. Plotted as the thin solid black line toward the lower part of each diagram is the prediction for the major merger fraction for galaxies from the Millennium simulation (Bertone & Conselice 2009). Also shown on these figures by the dotted blue line are the same predictions for major mergers as for warm dark matter models (e.g., Menci et al. 2012), which do a better job than CDM in matching the observed data. However, CDM better matches if minor mergers are taken into account, although the comparison merger fraction is only for major mergers based on the methodology used (Conselice et al. 2003a, Lotz et al. 2010a).

Other recent attempts to predict the merger history of observed galaxies include the abundance matching technique (e.g., Stewart et al. 2008), in which observed galaxies are matched to halos in models through their comparative abundance levels. Hopkins et al. (2010) predict, based on this abundance matching, the merger rate and fraction for galaxies. The result of this is shown in **Figure 12** for galaxies between $M_* = 10^{10-11}\,M_\odot$. Although the merger fractions from Hopkins et al. (2010) are higher than those from the CDM models, they are still lower than the observations [see also Jogee et al. (2009) and Lotz et al. (2011) for further discussions]. Similar results from Stewart et al. (2008) are also shown in **Figure 12**, who find results similar to those of Hopkins et al. (2010).

Finally, as a contrast to these, Maller et al. (2006) present cosmological hydrodynamical simulation results for similar mass galaxies of a few times $10^{10}\,M_\odot$ and find the highest merger fraction predictions of any simulation result (**Figure 12**). This shows that the predictions for merger histories are not correct or consistent with each other and that more simulation work should be focused on this critical aspect of the galaxy population. This is an area where future work is certainly needed.

There are several other types of simulations in which galaxy structure and morphology can be directly compared with observations of galaxies through cosmic time. Perhaps the most direct of these is to compare the properties and structural features of distant galaxies to hydrodynamical models of galaxy formation. Some of this work for galaxy mergers is discussed in Section 3.4. Early work in this area shows that the components of galaxies—namely bulges and disks—were the result of accretion events (e.g., Steinmetz & Navarro 2002), and these authors argued on the basis of their simulations that the Hubble type of a galaxy is not stable for long periods of cosmic time. Governato et al. (2007) show that disk galaxies having properties that match the morphological properties and kinematics of nearby disks can be simulated, although their simulation is not in a cosmological context. Overall, however, it is very difficult to predict the formation of galaxy morphology in simulations, and in a real sense this will be the ultimate test of galaxy formation models in the future.

Also, as discussed in Section 4.6, one of the most commonly seen properties in high-redshift star-forming galaxies is that they often contain large clumps of star formation within their disks. A major question is how these clumps form and evolve and how they may play a role in the formation of other galaxy components such as bulges and AGN. Bournaud et al. (2014) examined this problem computationally to determine how clumps with stellar masses of $M_* = 10^{8-9}\,M_\odot$ evolve in gaseous disks. The major question is whether these clumps dissipate within 50 Myr or so—which is the dynamical timescale of the clumps—or whether they regenerate and survive.

Bournaud et al. (2014) find that these clumps can last around 300 Myr by acquiring new gas from their disks, although some mass is lost through tidal effects. This is enough time to migrate toward the center of the galaxy, which can fuel the AGN or merge to form a bulge. This shows that these clumps may provide a significant route for galaxies to form. Thus, we have evidence for both inside-out and outside-in formation occurring in the galaxy population. What remains to be seen is whether one of these mechanisms is dominant as well as the relative role of both mechanisms in forming galaxies.

6. SUMMARY AND THE FUTURE

I present here a review of galaxy structure and morphology studies in the galaxy population through cosmic time from $z = 6$ until today. The approach taken in this review is largely observational with a limited amount of interpretation, although I do show where galaxy structure and morphology can test galaxy formation and even cosmological models in a new, largely unexplored way.

As of January 2014, the major conclusions concerning galaxy structure and its evolution, as discussed in this review, can be summarized by the following:

1. Galaxy structure and morphology are the longest-studied observational features of galaxies. In this review galaxy morphology is the apparent classification based on visual inspection, whereas structure is a way to quantify the light distributions in galaxies. In many ways, morphology is still a descriptive science, and visual efforts continue to provide useful information in the form of large-scale projects to classify many galaxies, as in the Galaxy Zoo effort. The Hubble sequence has and likely will remain the major paradigm in which we consider galaxy morphology, although this system does not "work" at high redshifts where most galaxies cannot be classified into a single Hubble type (Section 4.1).

2. Using the Hubble scheme, the evolution of three broad classes of galaxies is now classified accurately out to $z \sim 3$—namely ellipticals, spirals, and peculiars. The relative abundance of these galaxies has been measured as a function of redshift out to these early times. What we find is that the peculiar galaxies dominate the galaxy population at $z \sim 2.5$–3, and they have a relative fraction of at least 70%. Galaxies that are elliptical and spiral-like in appearance (but not necessarily in physical properties; see Section 4.1) become progressively more common at lower redshifts. The number densities of these two normal galaxy types together equal that of the peculiars by $z \sim 1.4$ (Mortlock et al. 2013).

3. Because galaxy morphology by visual estimates is limited in its ability to derive the physics behind galaxy formation and by its nature is not quantitative, the use of parametric (Section 2.2) and nonparametric (Section 2.3) methods is essential for deriving in a quantitative way how galaxies are evolving. These quantitative indices also correlate to some degree with the present and past star-formation history and properties of a galaxy. More work is needed to establish these relationships with more certainty, but it appears that the Sérsic index and concentration correlate with the scale or mass of a galaxy, the clumpiness index with the star formation, and the asymmetry parameter with ongoing merging activity (Section 3).

4. The merger history is now known from applying structural analyses to galaxy images in deep HST surveys such as the HDF (Section 4). The result is that the galaxy merger fraction increases with redshift at all stellar mass and luminosity selections. This increase can be fit well by a power law $(1+z)^m$ up to $z \sim 3$, although at higher redshifts the structurally derived merger fraction may plateau (Conselice & Arnold 2009). Using numerical/hydrodynamical simulations, the timescales for these mergers can be calculated, and thus merger fractions can be converted into merger rates (Section 4.3.2). The merger rate allows for the calculation of the number of mergers galaxies undergo at various masses as well as the amount of stellar

mass that is added to galaxies owing to the merger process. The result is that up to half of the stellar mass in modern massive galaxies was formed in mergers between $1 < z < 3$, although at $z < 1$ dry mergers are more likely responsible for the further formation of these galaxies.

5. The resolved structures of galaxies also allow us to measure the internal features of galaxies and how they are assembling. There is some controversy over the formation history of bulges, disks, and bars, although many of these are likely formed by secular processes produced internally by disk dynamical evolution. This is an area where significant progress could be made in the next few years. The most up-to-date results suggest that the bar fraction for spiral galaxies at $z < 1$ depends upon the stellar mass of the galaxy. The most massive galaxies have a similar bar fraction at $z \sim 0.8$ as they do today, yet lower-mass and bluer disk galaxies have a significantly lower bar fraction than similarly low-mass nearby disks. This mirrors the evolution of the Hubble sequence itself, where more massive galaxies settle into normal ellipticals and disks before lower-mass galaxies. Spiral structure is a difficult problem, and though some examples exist at high redshifts, even at $z > 2$, the general onset of when disks form spirals is almost totally unconstrained by observations.

6. Resolved imaging also permits us to measure the SEDs and colors of galaxy components and individual pixels of different galaxies. This is another area where more work needs to be performed, but it appears that bulges of spirals tend to be older than their disks at high redshift; there are examples of many ellipticals that have blue cores and central star formation (Section 4.4). Pixel-pixel analyses show that galaxies have a mixed star-formation history and that the inner parts of galaxies are often older than their outer parts. Pixel studies also show that the clumps seen in distant star-forming galaxies are composed of young stellar populations and thus must have recently formed or regenerated themselves.

7. Perhaps the most popular (at present) problem in galaxy structural evolution is the apparent compactness in size of galaxies at high redshifts. The observations show that massive galaxies at $z > 1$ have sizes that are a factor of 2–5 smaller than similar massive galaxies in today's Universe. This result has been studied in many different ways, and the sizes of a stellar mass–selected sample of galaxies increases gradually as a function of redshift with a power-law increase $\sim (1 + z)^{\beta}$, where β varies from -0.8 to -1.5 depending upon whether the selected samples are disk-like or elliptical-like (Section 4.2). Results to date suggest that these galaxies are building up their outer parts over time to become larger systems rather than adding mass to their centers. This process is unlikely driven by star formation, and theory suggests that this formation is produced by minor merger events (Section 4.2).

In summary, we have learned much about galaxy morphology and structure over the past 15 years. There are, however, many open questions still remaining on all aspects of using structure to determine evolution. More work needs to be done to tie galaxy structure to underlying physics, both through empirical work and in simulations. Furthermore, the timescales for structural features, such as mergers and large clump survival, are critical to achieve better understanding. Broad morphological features will remain important over the next decades as telescopes, such as the *James West Space Telescope*, *Euclid*, and the Large Synoptic Survey Telescope, and the Dark Energy Survey, among others, will all resolve many more galaxies than we can currently study, and they will do so at higher redshifts. This opens up entirely new possibilities, and with careful, thoughtful planning, a new revolution in galaxy structure may be upon us soon.

DISCLOSURE STATEMENT

ACKNOWLEDGMENTS

LITERATURE CITED

Abraham RG, Ellis RS, Fabian AC, Tanvir NR, Glazebrook K. 1999a. *MNRAS* 303:641
Abraham RG, Merrifield MR, Ellis RS, Tanvir NR, Brichmann J. 1999b. *MNRAS* 308:569
Abraham RG, van den Bergh S, Glazebrook K, et al. 1996. *Ap. J. Suppl.* 107:1
Abraham RG, van den Bergh S, Nair P. 2003. *Ap. J.* 588:218
Akiyama M, Minowa Y, Kobayashi N, et al. 2008. *Ap. J. Suppl.* 175:1
Allen PD, Driver SP, Graham AW, et al. 2006. *MNRAS* 371:2
Arp H. 1966. *Ap. J. Suppl.* 14:1
Barnes JE, Hernquist LE. 1991. *Ap. J.* 370:65
Barro G, Faber SM, Pérez-González PG, et al. 2013. *Ap. J.* 765:104
Bauer AE, Conselice CJ, Pérez-González PG, et al. 2011. *MNRAS* 417:289
Beckwith SVW, Stiavelli M, Koekemoer AM, et al. 2006. *Astron. J.* 132:1729
Bell EF, van der Wel A, Papovich C, et al. 2012. *Ap. J.* 753:167
Bendo GJ, Calzetti D, Engelbracht CW, et al. 2007. *MNRAS* 380:1313
Bershady MA, Jangren A, Conselice CJ. 2000. *Astron. J.* 119:2645
Bertone S, Conselice CJ. 2009. *MNRAS* 396:2345
Blanton MR, Moustakas J. 2009. *Annu. Rev. Astron. Astrophys.* 47:159
Bluck AFL, Conselice CJ, Almaini O, et al. 2011. *MNRAS* 410:1174
Bluck AFL, Conselice CJ, Bouwens RJ, et al. 2009. *MNRAS* 394:L51
Bluck AFL, Conselice CJ, Buitrago F, et al. 2012. *Ap. J.* 747:34
Blumenthal GR, Faber SM, Primack JR, Rees MJ. 1984. *Nature* 311:517
Bohm A, Wisotzki L, Bell EF, et al. 2013. *Astron. Astrophys.* 549:46
Bothun GD. 1986. *Astron. J.* 91:507
Bournaud F, Elmegreen BG, Elmegreen DM. 2007. *Ap. J.* 670:237
Bournaud F, Perret V, Renaud F, et al. 2014. *Ap. J.* 780:57
Bower RG, Benson AJ, Malbon R, et al. 2006. *MNRAS* 370:645
Bridge C, Appleton PN, Conselice CJ, et al. 2007. *Ap. J.* 659:931
Bruce VA, Dunlop J, McLure R, et al. 2012. *MNRAS* 427:1666
Buitrago F, Conselice CJ, Epinat B, et al. 2014. *MNRAS* 439:1494
Buitrago F, Trujillo I, Conselice CJ, et al. 2008. *Ap. J.* 687:L61
Buitrago F, Trujillo I, Conselice CJ, et al. 2013. *MNRAS* 428:1460
Bundy K, Ellis RS, Conselice CJ. 2005. *Ap. J.* 625:621
Buta RJ. 2013. In *Extragalactic Astronomy and Cosmology*, ed. TD Oswalt, WC Keel. *Planets, Stars and Stellar Systems*, 6:1–89. Dordrecht, Neth.: Springer
Calzetti D, Armus L, Bohlin RC, et al. 2000. *Ap. J.* 533:682
Caon N, Capaccioli M, D'Onofrio M. 1993. *MNRAS* 265:1013
Carollo M, Cibinel A, Lilly SJ, et al. 2013. *Ap. J.* 776:71
Carrasco ER, Conselice CJ, Trujillo I. 2010. *MNRAS* 405:2253
Cassata P, Giavalisco M, Williams CC, et al. 2013. *Ap. J.* 775:106
Chapman SC, Windhorst R, Odewahn S, Yan H, Conselice CJ. 2003. *Ap. J.* 599:92
Cohen JG, Cowie LL, Hogg DW, et al. 1996. *Ap. J.* 471:5
Cole S, Lacey CG, Baugh CM, Frenk CS. 2000. *MNRAS* 319:168

Combes F, Sanders RH. 1981. *Astron. Astrophys.* 96:164

Conroy C. 2013. *Annu. Rev. Astron. Astrophys.* 51:393

Conselice CJ. 1997. *Publ. Astron. Soc. Pac.* 109:1251

Conselice CJ. 2003. *Ap. J. Suppl.* 147:1

Conselice CJ. 2006a. *MNRAS* 373:1389

Conselice CJ. 2006b. *Ap. J.* 638:686

Conselice CJ. 2009. *MNRAS* 399:L16

Conselice CJ, Arnold J. 2009. *MNRAS* 397:208

Conselice CJ, Bershady MA, Dickinson M, Papovich C. 2003a. *Astron. J.* 126:1183

Conselice CJ, Bershady MA, Gallagher JS III. 2000a. *Astron. Astrophys.* 354:L21

Conselice CJ, Bershady MA, Jangren A. 2000b. *Ap. J.* 529:886

Conselice CJ, Blackburne J, Papovich C. 2005. *Ap. J.* 620:564

Conselice CJ, Bluck AFL, Buitrago F, et al. 2011b. *MNRAS* 413:80

Conselice CJ, Bluck AFL, Ravindranath S, et al. 2011a. *MNRAS* 417:2770

Conselice CJ, Bundy K, Trujillo I, et al. 2007. *MNRAS* 381:962

Conselice CJ, Chapman SC, Windhorst RA. 2003b. *Ap. J.* 596:L5

Conselice CJ, Gallagher JS, Calzetti D, Homeier N, Kinney A. 2000c. *Astron. J.* 119:79

Conselice CJ, Grogin N, Jogee S, et al. 2004. *Ap. J.* 600:L139

Conselice CJ, Morlock A, Bluck AFL, Grützbauch R, Duncan K. 2013. *MNRAS* 430:1051

Conselice CJ, Rajgor S, Myers R. 2008. *MNRAS* 386:909

Conselice CJ, Yang C, Bluck AFL. 2009. *MNRAS* 394:1956

Cooke J, Berrier JC, Barton EJ, Bullock JS, Wolfe AM. 2010. *MNRAS* 403:1020

Cooper MC, Griffith RL, Newman JA, et al. 2012. *MNRAS* 419:3018

Cotini S, Ripamonti E, Caccianiga A, et al. 2013. *MNRAS* 431:2661

Croton D, Springel V, White SDM, et al. 2006. *MNRAS* 365:11

Daddi E, Renzini A, Pirzkal N, et al. 2005. *Ap. J.* 626:680

Dahlen T, Mobasher B, Faber SM, et al. 2013. *Ap. J.* 775:93

Davis M, Efstathiou G, Frenk CS, White SDM. 1985. *Ap. J.* 292:371

Davis M, Guhathakurta P, Konidaris NP, et al. 2007. *Ap. J.* 660:L1

de Jong RS. 1996. *Astron. Astrophys.* 313:45

Delgado-Serrano R, Hammer F, Yang YB, et al. 2010. *Astron. Astrophys.* 509:78

De Propris R, Conselice CJ, Liske J, et al. 2007. *Ap. J.* 666:212

de Ravel L, Le Fèvre O, Tresse L, et al. 2009. *Astron. Astrophys.* 498:379

de Vaucouleurs G. 1948. *Ann. Astrophys.* 11:247

de Vaucouleurs G. 1959. *Handb. Phys.* 53:275

de Vaucouleurs G, de Vaucouleurs A, Corwin HG, et al. 1991. *Third Reference Catalogue of Bright Galaxies.*
    New York: Springer

Dickinson M. 2000. *Philos. Trans. R. Soc. Lond. Ser. A* 358:2001

Disney MJ, Romano JD, Garcia-Appadoo DA, et al. 2008. *Nature* 455:1082

D'Onghia E, Mapelli M, Moore B. 2008. *MNRAS* 389:1275

Dressler A. 1984. *Annu. Rev. Astron. Astrophys.* 22:185

Dressler A, Oemler A, Butcher HR, Gunn JE. 1994. *Ap. J.* 430:107

Driver SP, Windhorst RA, Ostrander EJ, et al. 1995. *Ap. J.* 449:L23

Dubinski J, Mihos JC, Hernquist L. 1999. *Ap. J.* 526:607

Dullo BT Graham AW. 2013. *Ap. J.* 768:36

Eggen OJ, Lyden-Bell D, Sandage AR. 1962. *Ap. J.* 136:748

Ellis RE. 1997. *Annu. Rev. Astron. Astrophys.* 35:389

Elmegreen BG, Bournaud F, Elmegreen DB. 2008. *Ap. J.* 688:67

Elmegreen BG, Elmegreen DM, Hirst AC. 2004. *Ap. J.* 612:191

Elmegreen DM, Elmegreen BG. 1987. *Ap. J.* 314:3

Elmegreen DM, Elmegreen BG, Ravindranath S, Coe DA. 2007. *Ap. J.* 658:763

Erb DK, Steidel CC, Shapley AE, et al. 2006. *Ap. J.* 646:107

Fang JJ, Faber SM, Koo DC, Dekel A. 2013. *Ap. J.* 776:63

Ferguson HC, Dickinson M, Giavalisco M, et al. 2004. *Ap. J.* 600:L107

Ferguson HC, Dickinson M, Williams R. 2000. *Annu. Rev. Astron. Astrophys.* 38:667

Ferrarese LCP, Jordán A. 2006. *Ap. J. Suppl.* 164:334

Finkelstein SL, Papovich C, Salmon B, et al. 2012. *Ap. J.* 756:164

Förster Schreiber NM, Genzel R, Bouche N, et al. 2009. *Ap. J.* 706:1364

Freeman PE, Izbicki R, Lee AB, et al. 2013. *MNRAS* 434:282

Gabor JM, Impey CD, Jahnke K, et al. 2009. *Ap. J.* 691:705

Genzel R, Burkert A, Bouche N, et al. 2008. *Ap. J.* 687:59

Giavalisco M, Ferguson HC, Koekemoer AM, et al. 2004. *Ap. J.* 600:L93

Giavalisco M, Livio M, Bohlin RC, Macchetto FD, Stecher TP. 1996. *Astron. J.* 112:369

Glazebrook K. 2013. *Publ. Astron. Soc. Aust.* 30:56

Glazebrook K, Ellis R, Santiago B, Griffiths R. 1995. *MNRAS* 275:19

Gomez PL, Nichol RC, Miller CJ, et al. 2003. *Ap. J.* 584:210

Governato F, Willman B, Mayer L, et al. 2007. *MNRAS* 374:1479

Graham AW. 2008. *MNRAS* 680:143

Graham AW. 2013. In *Extragalactic Astronomy and Cosmology*, ed. TD Oswalt, WC Keel. *Planets, Stars and Stellar Systems*, 6:91–140. Dordrecht, Neth.: Springer

Graham AW, Driver SP, Petrosian V, et al. 2005. *Astron. J.* 130:1535

Graham AW, Erwin P, Caon N, Trujillo I. 2001a. *Ap. J.* 563:11

Graham AW, Guzmán R. 2003. *Ap. J.* 125:2936

Graham AW, Scott N. 2013. *Ap. J.* 764:151

Graham AW, Trujillo I, Caon N. 2001b. *Astron. J.* 122:1707

Grogin NA, Conselice CJ, Chatzichristou E, et al. 2005. *Ap. J.* 627:L97

Grogin NA, Kocevski DD, Faber SM, et al. 2011. *Ap. J. Suppl.* 197:35

Grützbauch R, Chuter RW, Conselice CJ, et al. 2011a. *MNRAS* 412:2361

Grützbauch R, Conselice CJ, Varela J, et al. 2011b. *MNRAS* 411:929

Guo Q, White SDM, Boylan-Kolchin M, et al. 2011. *MNRAS* 413:101

Hambleton KM, Gibson BK, Brook CB, et al. 2011. *MNRAS* 418:801

Hathi NP, Ferreras I, Pasquali A, et al. 2009. *Ap. J.* 690:1866

Hernquist L, Katz, N. 1989. *Ap. J. Suppl.* 70:419

Hibbard J, Vacca WD. 1997. *Astron. J.* 114:1741

Holmberg E. 1958. *Lund Medd. Astron. Obs. Ser. II* 136:1

Holwerda BW, Munoz-Mateos J-C, Comeron S, et al. 2014. *Ap. J.* 781:12

Holwerda BW, Pirzkal N, de Blok WJG, et al. 2011. *MNRAS* 416:2401

Holwerda BW, Pirzkal N, de Blok WJG, Blyth S-L. 2013. *MNRAS* 435:1020

Holwerda BW, Pirzkal N, Heiner JS. 2012. *MNRAS* 427:3159

Hopkins PF, Bundy K, Murray N, et al. 2009. *MNRAS* 398:898

Hopkins PF, Croton D, Bundy K, et al. 2010. *Ap. J.* 724:915

Hopkins PF, Hernquist L, Cox TJ, Keres D. 2008. *Ap. J. Suppl.* 175:356

Hu J. 2008. *MNRAS* 386:2242

Hubble EP. 1926. *Ap. J.* 64:321

Hubble EP. 1936. *Realm of the Nebulae*. New Haven: Yale Univ. Press

Jiang L, Egami E, Fan X, et al. 2013. *Ap. J.* 773:153

Jogee S, Barazza FD, Rix H-W, et al. 2004. *Ap. J.* 615:L105

Jogee S, Miller SH, Penner K, et al. 2009. *Ap. J.* 697:1971

Joseph RD, Wright GS. 1985. *MNRAS* 214:87

Kartaltepe JS, Dickinson M, Alexander DM, et al. 2012. *Ap. J.* 757:23

Kartaltepe JS, Mozena M, Kocevski D, et al. 2014. *Ap. J.* Submitted. arXiv:1401.2455

Kartaltepe JS, Sanders DB, Scoville NZ, et al. 2007. *Ap. J. Suppl.* 172:320

Kaviraj S, Peirani S, Khochfar S, Silk J, Kay S. 2009. *MNRAS* 394:1713

Kaviraj S, Tan K-M, Ellis RS, Silk J. 2011. *MNRAS* 411:2148

Kennicutt R. 1998. *Annu. Rev. Astron. Astrophys.* 36:189

Kennicutt R, Evans NJ. 2012. *Annu. Rev. Astron. Astrophys.* 50:531

Kepple GR, Sanner GW. 1998. *The Night Sky Observer's Guide*, Vol. 1. Richmond, VA: Willmann-Bell
Khochfar S, Silk J. 2006. *Ap. J.* 648:21
Kocevski DD. 2012. *Ap. J.* 744:148
Kocevski DD, Faber SM, Mozena M, et al. 2012. *Ap. J.* 744:148
Koekemoer AM, Faber SM, Ferguson HC, et al. 2011. *Ap. J. Suppl.* 197:36
Koo DC, Kron RG. 1992. *Annu. Rev. Astron. Astrophys.* 30:613
Koo DC, Simard L, Willmer CNA, et al. 2005. *Ap. J. Suppl.* 157:175
Kormendy J. 1977. *Ap. J.* 217:406
Kormendy J. 1979. *Ap. J.* 227:714
Kormendy J, Bender R. 2012. *Ap. J. Suppl.* 198:2
Kormendy J, Djorgovski S. 1989. *Annu. Rev. Astron. Astrophys.* 27:235
Kormendy J, Drory N, Bender R, Cornell ME. 2010. *Ap. J.* 723:54
Kormendy J, Fisher DB, Cornell ME, Bender R. 2009. *Ap. J. Suppl.* 182:216
Kormendy J, Ho LC. 2013. *Annu. Rev. Astron. Astrophys.* 51:511
Kormendy J, Kennicutt R. 2004. *Annu. Rev. Astron. Astrophys.* 42:603
Kriek M, van Dokkum P, Franx M, et al. 2009. *Ap. J.* 705:71
Labbe I, Rudnick G, Franx M, et al. 2003. *Ap. J. Lett.* 591:L95
Lani C, Almaini O, Hartley WG, et al. 2013. *MNRAS* 435:207
Lanyon-Foster MM, Conselice CJ, Merrifield MR. 2007. *MNRAS* 380:571
Lanyon-Foster MM, Conselice CJ, Merrifield MR. 2012. *MNRAS* 424:1852
Law DR, Shapley AE, Steidel CC, et al. 2012a. *Nature* 487:338
Law DR, Steidel CC, Erb DK, et al. 2007. *Ap. J.* 656:1
Law DR, Steidel CC, Shapley AE, et al. 2012b. *Ap. J.* 759:29
Lee B, Giavalisco M, Williams CC, et al. 2013. *Ap. J.* 774:47
Le Fèvre O, Abraham R, Lilly SJ, et al. 2000. *MNRAS* 311:565
Lilly S, Carollo CM, Pipino A, Renzini A, Peng Y. 2013. *Ap. J.* 772:119
Lin L, Koo DC, Willmer CNA, et al. 2004. *Ap. J.* 617:L9
Lintott C, Schawinski K, Bamford S, et al. 2011. *MNRAS* 410:166
Lisker T. 2008. *Ap. J. Suppl.* 179:319
Lopez-Sanjuan C, Balcells M, Perez-Gonzalez PG, et al. 2010. *Ap. J.* 710:1170
Lopez-Sanjuan C, Le Fèvre O, de Ravel L, et al. 2011. *Astron. Astrophys.* 530:20
Lopez-Sanjuan C, Le Fèvre O, Ilbert O, et al. 2012. *Astron. Astrophys.* 548:7
Lotz JM, Davis M, Faber SM, et al. 2008a. *Ap. J.* 672:L177
Lotz JM, Jonsson P, Cox TJ, et al. 2011. *Ap. J.* 742:103
Lotz JM, Jonsson P, Cox TJ, Primack JR. 2008b. *MNRAS* 391:1137
Lotz JM, Jonsson P, Cox TJ, Primack JR. 2010a. *MNRAS* 404:575
Lotz JM, Jonsson P, Cox TJ, Primack JR. 2010b. *MNRAS* 404:590
Lotz JM, Primack J, Madau P. 2004. *Astron. J.* 128:163
Lundmark K. 1926. *Arkiv Mat. Astron. Fys.* 19(8):1–5
Madau P, Dickinson M. 2014. *Annu. Rev. Astron. Astrophys.* 52:415–86
Maller AH, Katz N, Keres D, Dave R, Weinberg DH. 2006. *Ap. J.* 647:763
Man AWS, Toft S, Zirm AW, et al. 2012. *Ap. J.* 744:85
Mannuci F, Cresci G, Maiolino R, et al. 2010. *MNRAS* 408:2115
McLure RJ, Pearce HJ, Dunlop JS, et al. 2013. *MNRAS* 428:1088
Menanteau F, Abraham RG, Ellis RS. 2001. *MNRAS* 322:1
Menci N, Fiore F, Lamastra A. 2012. *MNRAS* 421:2384
Meurer GR, Heckman TM, Leitherer C, et al. 1995. *Astron. J.* 110:2665
Mihos JC. 1995. *Ap. J.* 438:L75
Mihos JC, Hernquist L. 1996. *Ap. J.* 464:641
Moreno J, Bluck AFL, Ellison SL, et al. 2013. *MNRAS* 436:1765
Morgan WW. 1962. *Ap. J.* 135:1
Mortlock A, Conselice CJ, Bluck AFL, et al. 2011. *MNRAS* 413:2845
Mortlock A, Conselice CJ, Hartley W, et al. 2013. *MNRAS* 433:1185

Mosleh M, Williams RJ, Franx M, et al. 2012. 756:12

Naab T, Johansson PH, Ostriker JP. 2009. *Ap. J.* 699:178

Newman AB, Ellis RS, Bundy K, Treu T. 2012. *Ap. J.* 746:162

Noeske KG, Weiner BJ, Faber SM, et al. 2007. *Ap. J.* 660:43

Oesch PA, Bouwens RJ, Carollo CM, et al. 2010. *Ap. J.* 709:21

Oser L, Naab T, Ostriker JP, Johansson PH. 2012. *Ap. J.* 744:63

Ownsworth JR, Conselice CJ, Mortlock A, Hartley W, Buitrago F. 2012. *MNRAS* 426:764

Papovich C, Bassett R, Lotz JM, et al. 2012. *Ap. J.* 750:93

Papovich C, Dickinson M, Giavalisco M, Conselice CJ, Ferguson HC. 2005. *Ap. J.* 631:101

Papovich C, Giavalisco M, Dickinson M, Conselice CJ, Ferguson HC. 2003. *Ap. J.* 598:827

Patton DR, Pritchet CJ, Carlberg RG, et al. 2002. *Ap. J.* 565:208

Patton DR, Pritchet CJ, Yee HKC, Ellingson E, Carlberg RG. 1997. *Ap. J.* 475:29

Peletier RF, Balcells M. 1996. *Astron. J.* 111:2238

Peng CY, Ho LC, Impey CD, Rix H-W. 2002. *Astron. J.* 124:266

Peng Y, Lilly S, Kovac K, et al. 2010. *Ap. J.* 721:193

Peng Y, Lilly S, Renzini A, Carollo M. 2012. *Ap. J.* 757:4

Petrosian V. 1976. *Ap. J.* 209:L1

Postman M, Franx M, Cross NJG, et al. 2005. *Ap. J.* 623:721

Ravindranath S, Ferguson HC, Conselice CJ, et al. 2004. *Ap. J.* 604:L9

Ravindranath S, Giavalisco M, Ferguson HC, et al. 2006. *Ap. J.* 652:963

Reichard TA, Heckman TM, Rudnick G, Brinchmann J, Kauffmann G. 2008. *Ap. J.* 677:186

Ricciardelli E, Trujillo I, Buitrago F, Conselice CJ. 2010. *MNRAS* 406:230

Rix H-W, Zaritsky D. 1995. *Ap. J.* 447:82

Roberts MS. 1963. *Annu. Rev. Astron. Astrophys.* 1:149

Roberts MS, Haynes MP. 1994. *Annu. Rev. Astron. Astrophys.* 32:115

Sandage A. 1961. *The Hubble Atlas of Galaxies*. Washington, DC: Carnegie Inst.

Sandage A. 1975. *Galaxies and the Universe*, ed. A Sandage, M Sandage, J Kristian, p. 1. Chicago: Univ. Chicago Press

Sanders DB, Mirabel IF. 1996. *Annu. Rev. Astron. Astrophys.* 34:749

Savorgnan G, Graham AW, Marconi A, et al. 2013. *MNRAS* 434:387

Scarlata C, Carollo CM, Lilly S, et al. 2007. *Ap. J. Suppl.* 172:406

Schade D, Lilly SJ, Crampton D, et al. 1995. *Ap. J.* 451:L1

Scoville N, Aussel H, Brusa M, et al. 2007. *Ap. J. Suppl.* 172:1

Sellwood JA. 2014. *Rev. Modern Phys.* 86:1

Sérsic JL. 1963. *BAAA* 6:41

Shankar F, Marulli F, Bernardi M, et al. 2013. *MNRAS* 428:109

Shapley AE. 2011. *Annu. Rev. Astron. Astrophys.* 49:525

Shen S, Mo HJ, White SDM, et al. 2003. *MNRAS* 343:978

Sheth K, Elmegreen DM, Elmegreen BG, et al. 2008. *Ap. J.* 675:1141

Silk J, Mamon GA. 2012. *Res. Astron. Astrophys.* 12:917

Simard L, Meden JT, Patton DR, Ellison SL, McConnachie AW. 2011. *Ap. J. Suppl.* 196:11

Steidel C, Giavalisco M, Pettini M, Dickinson M, Adelberger KL. 1996. *Ap. J.* 462:17

Steinmetz M, Navarro JF. 2002. *New Astron.* 7:155

Stewart KR, Bullock JS, Wechsler RH, et al. 2008. *Ap. J.* 683:597

Strateva I. 2001. *Astron. J.* 122:1861

Swinbank AM, Smail I, Chapman SC, et al. 2010. *MNRAS* 405:234

Takamiya M. 1999. *Ap. J. Suppl.* 122:109

Targett TA, Dunlop JS, McLure RJ, et al. 2011. *MNRAS* 412:295

Tasca LAM, Kneib J-P, Iovino A, et al. 2009. *Astron. Astrophys.* 503:379

Tasca LAM, Le Fèvre O, Lopez-Sanjuan C, et al. 2014. *Astron. Astrophys.* 565:10

Taylor-Mager V, Conselice CJ, Windhorst R, Jansen R. 2007. *Ap. J.* 659:162

Toomre A, Toomre J. 1972. *Ap. J.* 178:623

Trujillo I, Conselice CJ, Bundy K, et al. 2007. *MNRAS* 382:109

van den Bergh S. 1960. *Ap. J.* 131:215

van den Bergh S. 1976. *Ap. J.* 206:883

van den Bergh S, Abraham RG, Ellis RS, et al. 1996. *Astron. J.* 112:359

van der Kruit PC, Freeman K. 2011. *Annu. Rev. Astron. Astrophys.* 49:301

van der Kruit PC, Searle L. 1982. *Astron. Astrophys.* 110:61

van Dokkum PG, Franx M, Kriek M, et al. 2008. *Ap. J.* 677:5

van Dokkum PG, Whitaker KE, Brammer G, et al. 2010. *Ap. J.* 709:1018

Weinzirl T, Jogee S, Conselice CJ, et al. 2011. *Ap. J.* 743:87

White SDM, Rees MJ. 1978. *MNRAS* 183:341

Williams CC, Giavalisco M, Cassata P, et al. 2014. *Ap. J.* 780:1

Williams RE, Baum S, Bergeron LE, et al. 2000. *Astron. J.* 120:2735

Williams RE, Blacker B, Dickinson M, et al. 1996. *Astron. J.* 112:1335

Windhorst RA, Taylor VA, Janse RA, et al. 2002. *Ap. J. Suppl.* 143:113

Wolf M. 1908. *Publ. Astrophys. Inst. Koenigstuhl-Heidelb.* 3:109

Wuyts S, Förster Schreiber NM, Genzel R, et al. 2012. *Ap. J.* 753:114

Zibetti S, Charlot S, Rix H-W. 2009. *MNRAS* 400:1181

Contents

Numerical Relativity and Astrophysics

Indexes

Errata

An online log of corrections to *Annual Review of Astronomy and Astrophysics* articles may be found at http://www.annualreviews.org/errata/astro